ENHANCING SUSTAINABLE CONSTRUCTION THROUGH LIME AND WATER HYACINTH ASH -MODIFIED COMPRESSED EARTH BLOCKS WITH IMPROVED ACOUSTIC PROPERTIES

BY

OUMA JUSTUS JUMA

A THESIS SUBMITTED IN PARTIAL FULFILMENT OF THE REQUIREMENTS FOR THE DEGREE OF MASTER OF SCIENCE IN PHYSICS

SCHOOL OF PHYSICAL AND BIOLOGICAL SCIENCES

MASENO UNIVERSITY

@ 2025

DECLARATION

I declare that this thesis is my own unaided work. It's being submitted in partial fulfillment of the Master of Science in Physics, School of Physical and Biological Science, Maseno University. It has not been submitted before for any other degree or examination in any other University.

Sign; …… Date; …….....

OUMA JUSTUS JUMA

MSC/SC/00019/019

This thesis has been submitted with our approval as supervisors;

Sign; …… Date; …….....

Prof. Andrew Odhiambo Oduor

Department of Physics and Material Science

Maseno University

Sign; …… Date; …….....

Dr. Erick Ogam

Research Engineer

Laboratory of Mechanics and Acoustics Marseille, France

ACKNOWLEDGEMENT

I would like to express the deepest appreciation to my supervisors Professor Andrew Oduor and Dr Erick Ogam who have the attitude and a substance of a genius: they continually and convincingly conveyed a spirit of adventure in regard to research and funding and an excitement in regard to teaching. Without their guidance and persistent help, this thesis would not have been possible.

Sincere thanks go to my research group members; Dr Nicholas Ongwen, Ms. Mercy Auma, Dr Z.E.A Fellah, Dr Mohammed Ben Mansour and Mr. Maxwel Mageto who played an important role during experimentation and analysis of the results.

I acknowledge the Department of Housing, Ministry of Lands, Busia County (Kenya) for providing the Hydra-form machine that was used in preparing the samples used in the study, Kenya Agricultural and Livestock Research Organization (KALRO), Alupe Centre, for providing soil analysis equipment and Kenya Medical Research Institute, Alupe Centre, for providing an incinerator.

Special thanks go to the French government through the Direction Europe de la recherche et coop′eration internationale (DERCI) AMOI-CNRS, in the framework of the Programme "Dispositif de Soutien aux Collaborations avec l ′ Afrique sub-saharienne, 2022–2024″ for funding this research.

DEDICATION

The Almighty God

ABSTRACT

Modern construction materials must meet a myriad of requirements, including sustainability, structural integrity, thermal efficiency, and acoustic performance. This study assesses the urgent need for eco-friendly construction materials by investigating the potential of using a blend of lime and water hyacinth ash (WHA) as binders in locally sourced soils from Mayenje ward, Busia County. The primary objective was to fabricate Compressed Soil-Lime-Water Hyacinth Ash (CSL-WHA) blocks with suitable acoustic absorption properties for sustainable building and construction. The specific objectives of this study were as follows; (i) To fabricate compressed earth blocks using a binder mixture of lime and water hyacinth ash, ensuring uniformity and structural integrity (ii) To evaluate the acoustical properties of CSL-WHA blocks by recovering key parameters through inverse modeling of transmission data (iii) To assess how binder ratios (lime vs. WHA) influence acoustic properties of CSL-WHA blocks and (iv) To examine the effect of compaction pressure on the acoustic properties of the blocks. The study delved into the feasibility of acoustical modeling for parameter retrieval, ultimately evaluating the potential of CSL-WHA blocks to meet specified acoustic requirements. A series of sixteen formulations were evaluated across four compaction pressures (25–100 bar) to assess the influence of binder composition and key acoustic parameters, including porosity, airflow resistivity, tortuosity, and viscous characteristic length. The results showed that moderate WHA ($\leq$5%) with high compaction pressure ($\geq$75 bar) could yield balanced porosity (~0.30–0.36) while achieving ideal air flow resistivity, tortuosity and viscous characteristic length ranges for sound absorption, striking a balance between acoustic performance and strength. Inverse modeling using the Johnson-Champoux-Allard-Lafarge (JCAL) framework enabled non-destructive recovery of intrinsic acoustic parameters. These findings offer a design matrix for balancing acoustic absorption and mechanical performance, supporting tailored applications in partition walls, facade systems, and low-frequency noise control. Furthermore, the study pioneers the valorization of invasive water hyacinth biomass for acoustic damping, providing a foundation for localized standardization and contributing to circular economy goals. The integration of WHA as a partial binder advances sustainable construction practices, reinforcing material innovation within environmental and acoustic design frameworks.

TABLE OF CONTENTS

DECLARATION ii
ACKNOWLEDGEMENT iii
DEDICATION iv
ABSTRACT v
TABLE OF CONTENTS vi
LIST OF ABBREVIATIONS AND ACRONYMS ix
LIST OF SYMBOLS xi
LIST OF TABLES xii
LIST OF FIGURES xiii
CHAPTER ONE:INTRODUCTION 1
1.1 Background of the study 1
1.1.1 Introduction 1
1.1.2 Rebirth of Eco-Friendly Compressed Earth Blocks 1
1.1.3 The Role of Binders in CEB Production 2
1.1.4 Cement's Environmental Impact 3
1.1.5 A Sustainable Alternative: Water Hyacinth Ash (WHA) 3
1.1.6 The Carbon-Neutral Potential of Lime 4
1.1.7 The Path to Reduced Costs and Emissions 6
1.1.8 The Emergence of Lime and WHA 7
1.1.8 Characterization of the soil 8
1.1.9 Understanding the Acoustic Properties 10
1.1.10 Acoustical modelling in porous media 13
1.1.11 Knowledge gap 17
1.2 Statement of the problem 17
1.3 Objectives of the study 18
1.3.1 General Objective 18
1.3.2 Specific Objectives 18
1.4 Research questions 19
1.5 Justification of the study 19
1.6 Significance of the study 21
1.7 Assumptions of the study 22
1.8 Limitations of the study 23

1.9 Scope of the study 25
CHAPTER TWO: LITERATURE REVIEW 26
2.1 Introduction 26
2.2 Water Hyacinth as a pozzolanic material 26
2.3 Lime as a binder in compressed soil blocks (CSBs) 29
2.4 Acoustic energy attenuation and characterization of air-saturated materials 30
2.5 The inverse identification 31
CHAPTER THREE:MATERIALS AND METHODS 33
3.1 Introduction 33
3.2 Research design 33
3.3 Raw materials 34
3.4 Mix-proportions for soil, lime, WHA and water 35
3.5 Preparation of the CSL-WHA blocks 36
3.6 Acoustic characterization of the CSL-WHA block 37
3.7 Solution of the inverse problem for the determination of acoustical parameters 39
CHAPTER FOUR:RESULTS AND DISCUSSIONS 42
4.1 Introduction 42
4.2 Characteristics of soils used 42
4.2.1 Granulometric analysis 42
4.2.2 Atomic Absorption Spectroscopy 42
4.3 Effect of WHA and lime concentrations on the acoustic transmission coefficient 44
4.4 The intrinsic acoustic parameters of the CSL-WHA blocks 46
4.5 Effect of concentration of WHA and lime on intrinsic acoustical properties 49
4.5.1 Porosity 50
4.5.2 Air flow resistivity 50
4.5.3 Tortuosity 51
4.5.4 Viscous characteristic length 51
4.5.5 Static thermal permeability 52
4.6 Effect of compaction pressure on the transmission coefficient 52
4.7 Effect of compaction pressure on intrinsic acoustical properties 53
CHAPTER FIVE:CONCLUSION AND RECOMMENDATION 55
5.1 Introduction 55
5.2 Conclusion 55

5.2.1 General Conclusion 55
5.2.2 Impact and Contribution of the Study 56
5.3 Recommendations 57
5.3.1 Possible applications 57
5.3.2 Further Investigation 58
REFERENCES 60
APPENDICES 74

LIST OF ABBREVIATIONS AND ACRONYMS

AAS	Atomic Absorption Spectroscoppy
AASHTO	American Association of State Highways and Transportation Officials
AFNOR	Association Francoise de Normalization (French Standardization)
ASTM	American Society for Testing and Materials
CAH	Calcium Aluminate Hydrates
CCUS	Carbon Capture Utilization and Storage
CEB	Compressed Earth Block
CSBs	Compressed Soil Blocks
CSEB	Compressed Stabilized Earth Block
CSH	Calcium Silicate Hydrates
CSL-WHA	Compressed Soil Lime and Water Hyacinth Ash
DAC	Direct Air Capture
DSO	Digital Storage Oscilloscope
EFM	Equivalent Fluid Model
EuLA	European Lime Association
GHG	Green House Gas
IP	Inverse Problem
LL	Liquid Limit
MDF	Medium Density Fibre
NASA	National Aeronautics and Space Administration
OPC	Ordinary Portland Cement
PI	Plasticity Index
PL	Plastic Limit
SLS	Sri Lanka Standard

T^{EFM}	Equivalent Fluid Model Transmission Coefficient
UN	United Nations
USGS	US Geological Survey
WHA	Water Hyacinth Ash

LIST OF SYMBOLS

α	Tortuosity
β	Compressibility
η	dynamic viscosity of air
k_o	Static permeability
k'_o	Thermal permeability
Λ	Viscous characteristic length
Λ’	Thermal characteristic length
ϕ	Porosity
P_r	Prandtl number
σ	Flow resistivity
$CaCO_3$	Calcium Carbonate
$Ca(OH)_2$	Calcium Hydroxide
CaO	Calcium Oxide
CO_2	Carbon dioxide
H_2O	Water
NOx	Nitric Oxide and Nitrogen dioxide

LIST OF TABLES

Table 1.1: Chemical properties of cement and WHA (Source: Das and Singh, 2016)..... 4

Table 1.2: Comparison of carbon dioxide emission and energy required for production of 1 tonne of cement and lime (Alireza & Mohsen, 2020 and EuLA, 2019.) 6

Table 1.3: Embodied Energy and CO2 emission for various types of earth blocks (Source: www.earth-auroville.com) 7

Table 3.1: Mix-proportions for soil, lime, WHA and water 35

Table 4.1: Granulometry 42

Table 4.2: Elemental composition of soil..... 43

Table 4.3: Values of the parameters obtained using IP for the CSL-WHA sample blocks at various densities 48

LIST OF FIGURES

Figure 1.1: Carbon neutral cycle of lime (Source: Campo, et al., 2021) 5

Figure 1.2: Mechanical shaker with a column of sieves used for sieve analysis (Source: *https://newarkwire.com/how-to-choose-the-right-test-sieve-shakers*) 8

Figure 3.1: Research framework for fabrication and acoustic characterization of CSL-WHA 33

Figure 3.2: (a) Fresh cut WH stems (b) The final WHA, ready for use; (c) The final sieved soil, ready for use; and (d) The prepared lime 35

Figure 3.3: (a) Mobile hydra-form block making machine (image taken at Busia County, department of housing); (b) Fabricated cylindrical mould for making CSL-WHA sample slabs; (c) The prepared CSL-WHA sample slabs for tests. 37

Figure 3.4: The experimental set up for the acoustic measurement of transmission coefficient of the samples 38

Figure 3.5: (a) Coiled waveguide (b) Ribbon loud speaker (c) Signal generator (d) Sub- woofer (e) Omnidirectional microphone (f) Pico scope 39

Figure 4.1: Transmission coefficient of the CSL-WHA samples at a pressure of 25 bars, with the soil at 90%. (a) 10% lime and 0% WHA; (b) 7% lime and 3% WHA; (c) 5% lime and 5% WHA; and (d) 3% lime and 7% WHA..... 44

Figure 4.2: Plots of cost functional Ƒ against the sought-for acoustical parameters for sample M-4: (a) Porosity (ϕ), (b) Airflow resistivity (σ), (c) Tortuosity ($\propto_\infty$), (d) Viscous characteristic length (Λ), (e) ratio (Λ'/Λ), and (f) thermal permeability ($\boldsymbol{k}_0'$). 47

Figure 4.3: Plots of the intrinsic acoustical parameters: (a) porosity, ϕ; (b) airflow resistivity σ; (c) tortuosity α_∞; (d) viscous characteristic length (e) the ratio between thermal characteristic length Λ' and viscous characteristic length Λ; (f) thermal permeability ($\boldsymbol{k}_0'$) against the sample number (from M-1 to M-4), all at a compaction pressure of 25 bars..... 49

Figure 4.4: Effect of compaction pressure on the acoustic transmission coefficient of the CSL-WHA (samples M-2, M-6, M-10 and M-14). 53

Figure 4.5: Plots of the intrinsic acoustical parameters: (a) porosity ϕ, and (b) airflow resistivity σ against compaction pressure. 53

CHAPTER ONE

INTRODUCTION

1.1 Background of the study

1.1.1 Introduction

Construction materials are increasingly expected to meet diverse requirements, including sustainability, structural integrity, thermal efficiency, and acoustic performance. In response to these demands, the versatility of a single material to meet all these criteria becomes crucial, as it saves time, money, energy, and space. Additionally, as global interest in sustainable building practices intensifies, the reduction of greenhouse gas emissions has emerged as a paramount concern (Gle` et al., 2011). This has prompted a resurgence in the use of eco-friendly compressed earth blocks (CEBs) for constructing affordable housing in both developed and developing countries (Piattoni et al., 2011).

1.1.2 Rebirth of Eco-Friendly Compressed Earth Blocks

The growing emphasis on sustainability has led to a resurgence in the utilization of eco-friendly compressed earth blocks (CEBs) for constructing affordable housing, addressing a challenge faced by both developed and developing countries (Lenci et al., 2012). The principal driver in this revival is the concern for the environment. The UN Climate Change Conference, Copenhagen, December 2009, confirmed the need to decrease carbon dioxide (CO_2) emissions by reducing the use of fossil fuels. The need to reduce CO_2 emissions and to find more sustainable construction materials has, for the time being, given earth construction a significant environmental advantage over some forms of conventional masonry (Williams et. al, 2010). The compressed earth blocks have the advantage of being constructed from local clays and soils that may be found on or close to the construction site, which contributes to their sustainability. For sustainable development, the Compressed Stabilized Earth Block (CSEB) provides the possibility for natural, energy-efficient, environmentally friendly, and agriculturally compatible building materials (Kamal, 2023).

The primary benefit of CSEB, especially for homes, is sustainability. CSEBs are an upgrade since they are cozy, cooler in the summer, and warmer in the winter. They use less energy to adjust the temperature when it has to be. They might easily adapt to exquisite, complex patterns. You can do whatever you want with the walls because they are weight bearing, only with some limitations (Powell, 2021).

CSEBs exhibit resistance to sound, fire, and insect damage, and they are durable when adequately protected (Arumala and Gondal, 2007). However, to ensure their structural integrity, optimization of material ingredients is crucial, especially concerning seismic events (Ocola and Huaco, 2005).

1.1.3 The Role of Binders in CEB Production

Producing CEBs involves a combination of soil and binders. Binders play a crucial role in enhancing the geotechnical properties of soil, including compressibility, strength, permeability, and durability. This is accomplished through chemical reactions between soil binder (cementitious material) and soil minerals (pozzolanic materials). Various types of binders, such as cement, lime, rice husks, fly ash, and blast furnace slag, have been explored for this purpose. Studies have indicated that addition of various stabilizing agents improved the workability of soils (Per and Pollina, 2023). Cement, a commonly used binding agent, poses environmental challenges due to its high carbon emissions and limited porosity. Sustainable alternatives, such as water hyacinth ash (WHA) and lime, have gained attention for their potential to reduce costs and emissions (Alavez-Ramirez et.al 2012, Philip and Rakendu, 2020). Lime application results in an increase in strength due to cation exchange capacity rather than cementing effect caused by pozzolanic reaction. WHA is a promising pozzolanic compound with its mineralogical composition comparable to cement, hence can be used as a replacement for cement (Das and Singh, 2016).

1.1.4 Cement's Environmental Impact

While cement has traditionally been the go-to binding agent due to its versatility in various soil types, its production, particularly the precursor clinker, contributes significantly to global carbon dioxide (CO_2) emissions. According to NASA (2020), one of the main greenhouse gas emitters and a primary cause of global warming is CO_2. In 2017, the world's cement production generated 4.1 gigatons of CO_2 (USGS, 2018). Therefore, anthropogenic climate change may become inevitable due to such high CO_2 levels. Furthermore, throughout the extraction, packaging, and loading stages of the cement manufacturing process, particulate matter of diameters 2.5 micrometres (PM2.5) and 10 micrometers (PM10) is emitted (Mishra and Saddiqui, 2014). These particles pose a serious health risk because they can penetrate deep into the lungs and even enter the bloodstream. Consequently, one tonne of Portland cement generates approximately one tonne of greenhouse gas (GHG), and 1.5 to 10 kg of Nitrogen Oxides (NOx) is released into the atmosphere for every tonne of Portland cement clinker (Malhotra, 2004). NOx is a strong greenhouse gas produced by burning biomass, nitric acid synthesis, and fossil fuels (NASA, 2020). Moreover, walls constructed with cement as a binder lack porosity, making them less efficient in terms of thermal and acoustic insulation, consequently requiring more energy for climate control. In this study, cement as a binder is replaced with an eco-friendly binder, the hydrated lime, in the manufacture of construction blocks.

1.1.5 A Sustainable Alternative: Water Hyacinth Ash (WHA)

To address the challenges caused by cement production and use, there has been a growing trend in recent decades of blending ordinary cement and lime with locally sourced materials possessing pozzolanic properties, for the production of concrete and compressed soil blocks.

Water hyacinth is a free-floating aquatic plant that grows in still or slow-moving fresh water bodies. Within two weeks, the number of water hyacinths doubles, and it grows quickly, producing a considerable amount of biomass hence, it is a sustainable product (Shyam & Murugesh, 2017). WHA has pozzolanic properties, and its production cost is low. Its

mineralogical composition includes reactive phases akin to those in cement, allowing it to act as a sustainable binder in compressed soil blocks with added benefits of lower carbon emissions and reduced energy input.

Table 1.1: Chemical properties of cement and WHA (Source: Das and Singh, 2016)

Chemical composition	Cement (%)	WHA (%)
Silica	19.62	4.40
Alumina	5.62	2.20
Iron Oxide	5.33	1.27
Calcium Oxide	61.24	22.61
Magnesia	0.88	14.01
Sulphur Trioxide	2.60	3.09
Sodium Oxide	-	0.35
Potassium Oxide	-	14.82

1.1.6 The Carbon-Neutral Potential of Lime

The use of hydrated lime, although emitting carbon dioxide during the burning phase, has the unique ability to reabsorb equivalent amounts of carbon dioxide from the atmosphere, resulting in a carbon-neutral life cycle. The unstable calcium oxide allows a variety of lime- based products, including wastes produced in different industries, to absorb some of the emitted CO_2 and subsequently sequester it throughout the lime cycle (carbonation) (Cizer et. al., 2012a, Campo, et al., 2021).

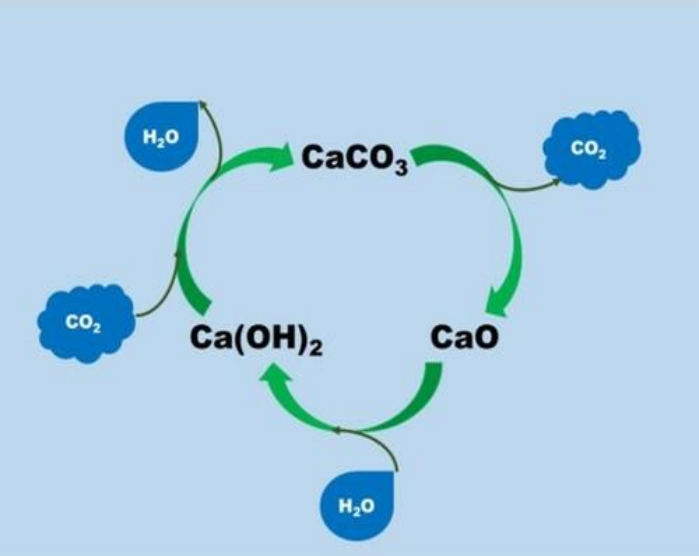


Figure 1.1: Carbon neutral cycle of lime (Source: Campo, et al., 2021)

Renforth (2019) estimates that 34% of lime has the ability to absorb CO_2 throughout the use stage and remove it from the atmosphere directly or indirectly. The following reactions can be used to describe the carbonation process:

$$Ca\,O + H_2O \longrightarrow Ca\,(OH)_2 \quad 1.1$$

$$Ca\,(OH)_2 + CO_2 \longrightarrow CaCO_3 + H_2O \quad 1.2$$

Carbonation is a mineralization process that is used for carbon capture, utilization, and storage (CCUS) (Lai et al., 2021; Snaebjörnsdóttir et al., 2020). It happens gradually from the outside to the inside of materials that contain lime due to the diffusion of CO_2 into particles and its reaction with calcium oxide hydration products. Solid sorbents composed of materials derived from lime have been suggested for application in direct air capture (DAC) technologies, which collect CO_2 directly from the atmosphere, according to Samari et al. (2020). However, in reality, approximately 70%–80% of the CaO in lime can be transformed into $CaCO_3$ due to material and environmental variables (Bhatia and Perlmutter, 1983). Prior studies have examined the carbonation process, factors influencing its rate (Ma et al., 2019), and strategies for optimizing carbon sequestration in controlled laboratory environments through the use of materials

containing lime (Pan et al., 2012; Baciocchi, 2017).

For example, Pan et al. (2020) examined the potential for CO_2 storage in solid wastes composed of lime (such as lime mud, red mud, and iron and steel slags) and the CO_2 reduction potential of these wastes in mineralization technologies. By using direct mineralization, these solid wastes can carbonate up to a maximum of 310Mt of CO_2 annually. Renforth (2019) estimated the global potential of carbon dioxide uptake through the carbonation of lime and related alkaline minerals up to the year 2100, (roughly 2.9-8.5Gt of CO_2 per year), and he found that this process can significantly reduce CO_2 emissions during the production of the related materials.

1.1.7 The Path to Reduced Costs and Emissions

Fabrication of CSL-WHA blocks presents an opportunity for cost reduction in construction, a decrease in greenhouse gas emissions, and reduced energy input, contributing to the fight against global warming. Lime, in particular, offers the flexibility to work with a wider range of natural soils, eliminating the need for sand or quarry dust blending, which is often associated with cement. This transition is even more compelling when considering the significant energy consumption and CO_2 emissions associated with cement and lime production, as highlighted in Table 1.2.

Table 1.2: Comparison of carbon dioxide emission and energy required for production of 1 tonne of cement and lime (Alireza & Mohsen, 2020 and EuLA, 2019.)

Material	CO_2 emissions (tonnes)	Energy emission (GJ)
Cement	0.99	3.4
Lime	0.751	3.18

The complete re-use and biodegradability of these blocks at the end of their useful life in the earth's structure is also very important. Unfired earth blocks offer a significantly more sustainable alternative to fired bricks, requiring substantially less embodied energy during production and releasing up to 80% less carbon dioxide into the atmosphere. Thus, the use of eco-friendly binders like Lime and WHA in manufacture of compressed soil blocks (CSB) minimizes CO_2 emissions

and its associated negative environmental impacts (Nagaraj et. al, 2014). Furthermore, as opposed to fired earth blocks, unfired earth blocks have low production costs. A comparison of energy and CO_2 emissions between various block types underscores the benefits of compressed soil blocks (CSBs) with binders, which emit significantly less CO_2 and require lower embodied energy for production (Table 1.3).

Table 1.3: Embodied Energy and CO2 emission for various types of earth blocks (Source: www.earth-auroville.com)

Type	Initial embodied energy per m^3 of wall	Pollution emission (kg of CO2) per m^3 of wall
CSB	631 MJ/m^3	56.79 kg/m^3
Kiln fired block	2356 MJ/m^3	230.06 kg/m^3
Country fired block	6358 MJ/m^3	547.30 kg/m^3

In contrast to concrete and steel structures, which are expensive and require skilled labor, CSBs offer an economical choice for construction. Their production involves simplicity and affordability.

1.1.8 The Emergence of Lime and WHA

In recent decades, the combination of lime and locally sourced materials with pozzolanic properties has gained traction for making compressed soil blocks (Nagaraj H. B., et al., 2014, 2016). Lime offers flexibility in soil selection and exhibits carbon-neutral properties during its life cycle (Alavez-Ramirez et al., 2012). WHA is a promising pozzolanic compound with its mineralogical composition comprising of reactive phases akin to cement (Table 1.1) hence can be used as a replacement for cement (Das and Singh, 2016). The context of using WHA is beneficial in terms of cost- efficiency, reduced greenhouse gas emissions, and improved insulation.

1.1.8 Characterization of the soil

(a) Granulometric analysis using sieve test method

A sieve analysis is a practice or procedure used to assess the particle size distribution (also called *gradation*) of a granular material by allowing the material to pass through a series of sieves of progressively smaller mesh size and weighing the amount of material that is stopped by each sieve as a fraction of the whole mass. A typical sieve analysis involves a nested column of sieves with wire mesh cloth (screen). The column of sieves is used in a mechanical shaker.

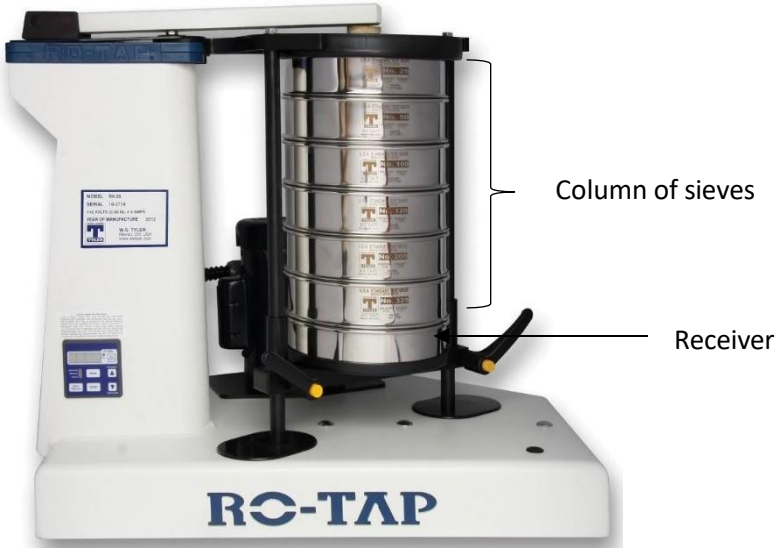


Figure 1.2: Mechanical shaker with a column of sieves used for sieve analysis (Source: *https://newarkwire.com/how-to-choose-the-right-test-sieve-shakers*)

Poured into the top sieve, which has the greatest screen opening, is a representative weighed sample. The apertures in each column's lower sieve are smaller than those in the upper sieve. The receiver is a circular pan located at the base. Usually, the column is set up in a mechanical shaker. The column is shaken by the shaker, usually for a predetermined period of time. The material on the sieve is weighed when the shaking is finished. The mass of the sample of each sieve is then divided by the total mass of the soil sample to give the percentage retained on each sieve. The soil is then characterized as gravels, sand, clay and silt, depending on the diameters of the particles as retained on the respective sieves. The results of this test are used to describe the properties of the

aggregate and to see if it is appropriate for various civil engineering purposes.

(b) Atomic Absorption Spectroscopy (AAS)

Atomic Absorption Spectroscopy (AAS) is a well-established analytical technique used for the quantitative determination of metal elements in various matrices, including soils, industrial waste, and construction materials. Developed in the mid-20th century, AAS has become a cornerstone in environmental monitoring, geochemical analysis, and materials characterization due to its precision, sensitivity, and elemental specificity (Visser, D., 2024).

The fundamental principle of AAS is based on the absorption of light by free atoms in the ground state. When a sample is atomized, typically using a flame or graphite furnace, the atoms absorb radiation at wavelengths unique to each element. The extent of absorption is directly proportional to the concentration of the element in the sample, enabling accurate quantification even at trace levels (Malhotra, 2023).

In the context of sustainable construction, particularly in the development and optimization of compressed soil-lime blocks (CSL-WHA), AAS serves multiple critical function. It facilitates the characterization of raw soil by identifying key metallic constituents, such as iron (Fe), calcium (Ca), magnesium (Mg), and aluminum (Al), as well as aluminium oxide and silicon dioxide, which influence pozzolanic reactions and binder performance. Additionally, AAS enables the detection of potentially hazardous metals, including lead (Pb), cadmium (Cd), chromium (Cr), and nickel (Ni), ensuring that materials meet environmental safety standards for residential and public infrastructure applications.

The technique's high sensitivity (often reaching parts per billion) and ability to selectively analyze individual elements make it particularly suitable for evaluating the suitability of locally sourced materials in resource-constrained settings. Moreover, AAS data can be integrated into broader sustainability assessments, including life cycle analysis and carbon footprint evaluations, thereby supporting evidence-based decision-making in eco-friendly construction practices.

Despite its advantages, AAS is limited to the analysis of metallic elements and requires careful sample preparation, including acid digestion and calibration with certified standards. Nonetheless, its robustness and reliability continue to make it a preferred method in both academic research and industrial quality control.

In this study, AAS is employed to assess the elemental composition of soil samples intended for use in CSL-WHA block production. The findings inform material selection, binder formulation, and environmental compliance, contributing to the overarching goal of developing scalable, carbon-neutral construction solutions.

1.1.9 Understanding the Acoustic Properties

CSL-WHA blocks are porous materials with specific acoustic parameters that govern sound absorption and reduction indices. The primary factors influencing the sound absorption and sound reduction indices are the viscous characteristic length, porosity, airflow resistivity, and tortuosity (Allard and Atalla, 2009).

Air flow resistivity, (σ): The flow resistivity of porous material is defined as the ratio between the pressure difference across a sample and the velocity of flow of air through that sample per unit cube. Materials with low resistivity tend to transmit sound more easily, while those with higher resistivity exhibit better sound absorption due to enhanced viscous damping. Understanding and controlling airflow resistivity is therefore essential for designing multi- functional compressed soil blocks that meet both structural and acoustic performance criteria. Studies by Ben Mansour et al. (2016) and Ongwen & Alruqi (2023) have shown that airflow resistivity values between 15,000 and 35,000 Pa·s/m² strike a balance between acoustic damping and mechanical strength.

Porosity, (ϕ): Is a fraction of the volume of voids over the total volume (Allard and Atalla, 2009). The acoustic porosity is the open porosity, meaning that only those pores that can be accessed from the outside contribute to the porosity. Closed cells should not be taken into account, they have only an effect on the apparent density and elasticity of the frame.

$$\phi = \frac{V_a}{V_T} \quad 1.3$$

where V_a is the volume of air saturating the material, excluding closed pores and V_T is the total volume of the material.

Studies have consistently shown that the porosity range influences not only the airflow resistivity and absorption coefficients but also the structural integrity of the blocks. Ben Mansour et al. (2016) identified that CEBs fabricated under varying compaction pressures exhibit porosity values between 0.25 and 0.35. Building on this, Ben Mansour et al. (2017) found that porosity values between 0.26 and 0.34 yielded favorable acoustic absorption while ensuring a compressive strength above 2 MPa. Earlier work by Adam and Jones (1995) corroborated this trend, observing that stabilized blocks maintained effective thermal conductivity and structural performance at porosity levels around 0.30. These findings highlight the importance of targeting a porosity range of approximately 0.25 to 0.35 in sustainable construction applications, particularly where acoustic absorption and structural performance must be optimized simultaneously.

Tortuosity, ($\propto$): Is the ratio of actual flow path length to the straight distance between the ends of the flow path. The classical tortuosity is given in equation 1.6 when the frame is saturated by an ideal non viscous fluid.

$$\propto_\infty = \frac{\rho}{\rho_o} \quad 1.4$$

where ρ is the effective density of the porous medium, ρ_o is the density of air, and $\propto_\infty$ is the classical tortuosity.

The micro geometry of the porous material determines the tortuosity. In engineered materials such as compressed soil blocks, when stabilized with lime and cement a moderate tortuosity range has been shown to support the dual objective of efficient sound attenuation and sufficient load bearing capacity. Holtzer et. al 2023 observed that for simple microstructures**,** such as packed spheres and

ellipsoids, the corresponding data points are in a narrow band close to and often slightly above the Bruggeman trend line… typically <2.0, indicating that tortuosity values below 2 are characteristic of well-structured porous systems. These findings substantiate the relevance of a target range between 1.4 and 2.0, which aligns with empirical observations in stabilized CSBs and reflects an optimal balance between acoustic permeability and material consolidation.

Viscous characteristic length, (Λ): Viscous characteristic length is a parameter related to the effective density of the porous material and can be interpreted as representing viscous attenuation caused by the movement of the air in narrow voids. Experimental studies have shown that CSBs with Λ values between 80–150 μm tend to strike a balance between acoustic absorption and compressive strength (Brown et al., 1996). For example, Ben Mansour et al. (2016) recovered Λ values in the range of 90–130 μm for blocks compacted at moderate pressure, correlating with favorable transmission loss and structural integrity

Describing porous media acoustically necessitates consideration of 1 to 8 parameters, contingent upon the material's microstructure. Among these, the static airflow resistivity (σ) stands out as a pivotal metric, particularly for acoustical porous materials characterized by high open porosities (ϕ). Functioning as a key indicator of viscous losses and acoustic energy attenuation within the low-frequency range, σ assumes paramount importance in this domain. Its significance lies in its unique ability to encapsulate the delicate equilibrium between airflow and acoustic energy, making it fundamental to understanding porous materials' behavior in acoustical contexts.

For acoustical porous materials boasting high open porosities (ϕ), the static airflow resistivity (σ) takes precedence. It can be directly measured, with ISO 9053 (1991) providing a dedicated standard for its assessment. Alternatively, it can be derived from the material's low-frequency behavior, where viscous effects dominate all other influences.

In addition to porosity (ϕ), which can be directly measured, other acoustical parameters lack standardized assessment methods. These parameters include the high-frequency limit of the

dynamic tortuosity (the viscous characteristic length (Λ), the thermal characteristic length (Λ'), the static thermal permeability (k'), and the low-frequency limits for the viscous and thermal tortuosities ($\propto_o$ and $\propto'$) Estimating the latter two parameters is particularly challenging, often relying on model fitting to measurements (Panneton and Olny, 2006). In this study, we employed methods based on the measurement of reflection and transmission coefficients at audible frequencies in an impedance tube to estimate σ, ϕ, α_∞, k',, Λ, and Λ'.

1.1.10 Acoustical modelling in porous media

Within the realm of porous media studies, two primary scenarios often arise. When acoustic attenuation stems from combined influences of the fluid and solid phases, the Biot model serves as the go-to framework for describing wave propagation within both mediums (Biot, 1956). This model elucidates the emergence of two compressional waves and one rotational wave.

However, a more straightforward method using an equivalent fluid model is frequently used in porous media saturated with air, where the solid structure can be thought of as inflexible and its vibrations as insignificant. This model only considers the compressional wave propagation in the fluid phase of the porous medium.

In order to faithfully represent the complex interaction between the solid and fluid structures inside the pores, classical attributes such as compressibility and density are replaced with their corresponding values. Visco-inertial and thermal fluid-structure interactions can be included with this modification.

Various models have been developed to describe these exchanges comprehensively. Here, we explore the intricacies of the most sophisticated models, delving deeper into their mechanisms and implications.

a. The model of Johnson et al. for the dynamic tortuosity

Johnson et al. (1987) proposed a simple model describing the function α(ω), which is the dynamic tortuosity, when the porous structure is saturated with a Newtonian viscous fluid. This model can be applied to the case of our porous structures saturated with air.

Two model parameters, the tortuosity α_∞ and the viscous characteristic length Λ are involved in a high- frequency limit:

$$\propto(\omega) = \propto_\infty \left(1 - \frac{2}{\Lambda}\left(\frac{\eta}{j\omega\rho_f}\right)^{1}/_{2}\right) \qquad \omega \to \infty \tag{1.5}$$

where$j^2 = -1$, η is the dynamic viscosity of the fluid, ω the angular frequency, ρ_f the density of the fluid. In the low frequency limit, the expression of the dynamic tortuosity in the frequency domain is given by (Johnson et al., 1987):

$$\propto(\omega) = -\frac{\eta\phi}{\rho_f k_o j\omega'} \qquad \omega \to 0 \tag{1.6}$$

where k_o is the viscous permeability given by: $k_o = \frac{\eta}{\sigma}$ (with the dimension of a surface), σ is the specific resistance passage of the fluid. The meaning of the quantities $\propto_\infty, \Lambda, k_o$ have been given previously. Johnson et al. 1987 imply that these three geometric parameters provide sufficient information about the microgeometry. The proposed general expression for $\propto(\omega)$ is then that of the simplest analytic function verifying these limits:

$$\propto(\omega) = \propto_\infty \left(1 - \frac{1}{jx}\sqrt{1 - \frac{M}{2}jx}\right) \quad \text{where } x = \frac{\omega \propto_\infty \rho f}{\sigma\emptyset} \text{ and } M = \frac{8k_o \propto_\infty}{\emptyset\Lambda^2} \tag{1.7}$$

b. The dynamic compressibility equivalent model

Given the importance of the solid part's heat capacity, a model akin to the prior one has been established for the frequency dependence of thermal exchanges between the fluid and the structure. The final result is a two-parameter model, referred to as Λ' and k′ 0/φ, where λ and k0 stand for the respective roles that viscous and thermal effects play. According to Allard and Champoux (1991), β(ω) behaves as follows in a high-frequency limit:

$$\beta(\omega) = 1 - \frac{2(\gamma-1)}{\Lambda'}\left(\frac{\eta}{P_r\rho_f}\right)^{1}/_{2}\left(\frac{1}{j\omega}\right)^{1}/_{2} \qquad \omega \to \infty \tag{1.8}$$

where γ is the adiabatic constant and P_r is the number of Prandtl. As previously mentioned, this trend suggests that the thickness of the thermal boundary layer decreases in relation to any

characteristic radius of curvature of the interface. It is evident that the tortuosity $\propto_\infty$ for thermal effects has no equivalent; at very high frequencies, β(ω) tends to 1 as ∝(ω) goes to the tortuosity $\propto_\infty$.

Lafarge et al. (1996) demonstrated that, at the low frequency limit:

$$\beta(\omega) = \gamma + \frac{(\gamma-1)\rho_f k_o' P_r}{\eta\phi j\omega}, \quad \text{when } \omega \to 0 \tag{1.9}$$

here k_o', is a parameter similar to k_o but tailored to the thermal problem, has the same size (area) as the Darcy permeability of k_0. The general formula for β(ω) that has been suggested is one of the most basic analytic function that satisfies the limits of 1.8 and 1.9.

$$\beta(\omega) = \gamma - \frac{\gamma-1}{1-\frac{1}{jx'}\sqrt{1-\frac{M'}{2}jx'}} \text{ where } x' = \frac{\omega\rho f k_{oPr}'}{\eta\phi} \text{ and } M' = \frac{8k_o'}{\phi\Lambda'^2} \tag{1.10}$$

the parameter k_o' introduced by Lafarge et. al 1997 termed, by analogy with viscous permeability, thermal permeability.

c. Model extensions by Pride and Lafarge

Johnson et al. 1987 development in high frequency for the tortuosity dynamics ends with the term $\frac{\mathbf{1}}{\sqrt{\boldsymbol{j\omega'}}}$. A second correction term $\frac{\mathbf{1}}{\boldsymbol{j\omega}}$, was presented by Pride et al. in 1993. The dynamic tortuosity's asymptotic expansion is currently expressed as follows:

$$\propto(\omega) = \propto_\infty \left(1 - \frac{2}{\Lambda}\left(\sqrt{\frac{\eta}{j\omega\rho_f}}\right) - \frac{\sigma\phi(1-\wp)}{j\omega\rho_{f\propto_\infty}}\right); \omega \to \infty \tag{1.11}$$

The Pride parameter, $\wp$, is a dimensionless geometrical parameter that is linked to a correction term, $\propto_0$, which functions as the fluid's inertia at low frequencies;

$$\wp = \frac{M}{4(\frac{\propto_o}{\propto_\infty}-1)} \qquad M = \frac{8k_o\propto_\infty}{\phi\Lambda^2}$$

Below is the expansion of dynamic tortuosity at low frequency;

$$\propto(\omega) = -\frac{\eta\phi}{\rho_f k_o jw} + \propto_o, \qquad \omega \to 0 \tag{1.12}$$

The updated formulation of the analytic function, which incorporates the advancements of (1.13) and (1.14), is as follows:

$$\propto(\omega) = \propto_{\infty} \left(1 - \frac{1}{jx}\left(1 - \wp + \wp\sqrt{1 - \frac{M}{2\wp^2}jx}\right)\right) \quad 1.13$$

The value of $\wp$ is dependent on the geometry of the pores; for instance, it can be demonstrated that $\wp = {}^{3}/_{4}$ in the case of circular-section cylindrical pores. For rectangular parts, values near ${}^{3}/_{4}$ are obtained.

Similar formulation for the dynamic thermal compressibility was presented by Lafarge (1996), who corrected the Allard and Champoux model for higher frequencies and included a dimensionless parameter $\wp'$. Subsequently, the dynamic compressibility expression is provided by:

$$\beta(\omega) = 1 - (\gamma - 1)\left[\frac{2}{\Lambda'}\left(\sqrt{\frac{\eta}{P_r\rho_f}}\right)\left(\sqrt{\frac{1}{j\omega}}\right) + \left(\frac{\eta}{\rho_f P_r j\omega}\right).\left(\frac{(1-\wp')\phi}{k_0'} - \frac{4}{\Lambda'^2}\right)\right] \quad \omega \to \infty \quad 1.14$$

The fluid's low-frequency thermal inertia is described by $\propto_o'$, the thermal equivalent of $\propto_o$ and is related to the parameter $\wp'$:

$$\wp' = \frac{M'}{4(\propto_o' - 1)}$$

The dynamic compressibility's general expression is given by:

$$\beta(\omega) = \gamma - (\gamma - 1)/\left[1 - \frac{1}{jx'}\left(1 - \wp' + \wp'\sqrt{1 - \frac{M'}{2\wp'^2}jx'}\right)\right] \quad 1.15$$

It can be observed that when $\wp = 1$ and $\wp' = 1$, the Pride and Lafarge models are narrowed down to those of Johnson and Allard.

1.1.11 Knowledge gap

Despite the rising interest in utilizing Water Hyacinth Ash (WHA) as an alternative to Ordinary Portland Cement (OPC), the existing literature lacks evidence regarding its effectiveness as a binder when combined with lime to create Compressed Soil Blocks (CSBs) meeting the necessary acoustical standards in construction practices.

Moreover, while lime can be used in conjunction with cement, it is crucial to acknowledge that cement, from an environmental perspective, is unsustainable. Therefore, exploring the potential of lime in combination with a locally available eco-friendly cementitious material like WHA for the production of construction blocks is not only pertinent but also aligns with sustainable practices. This research avenue holds promise for both environmental conservation and the development of acoustically viable construction materials.

1.2 Statement of the problem

In the face of escalating global concerns about sustainable construction practices, the urgent need to curtail greenhouse gas emissions has taken center stage. Cement, as the predominant construction material, not only incurs high production costs but also poses severe environmental challenges. Its production, notorious for emitting significant amounts of CO_2, exacerbates the menace of global warming. A staggering 0.99 tonnes of CO_2 are generated per tonne of cement produced; a fact underscored by the high-temperature processes required for clinker formation. The consequence is a substantial release of CO_2 into the atmosphere, contributing significantly to climate change.

The environmental quandary is compounded by the inherent inefficiency of cement-based walls. Lacking porosity, these walls fail to offer optimal thermal and acoustic insulation, demanding higher energy consumption for climate control. To mitigate construction costs, energy usage, and CO_2 emissions, a growing trend involves mixing of Portland cement (OPC) with pozzolanic elements that can be found locally, like Water Hyacinth Ash (WHA), or replacing it entirely with

more energy-efficient binders like hydrated lime. This has led to the development of Compressed Stabilized Lime-Water Hyacinth Ash (CSL-WHA) blocks, representing a promising eco-friendly alternative.

However, the challenge lies in ensuring these innovative construction materials meet the trifecta of requirements: structural integrity, thermal efficiency, and acoustic performance. While numerous studies have delved into the mechanical and thermal properties of these blocks; the acoustical aspects have been significantly overlooked. This gap in research emphasizes the pressing need to delve into the intrinsic acoustic parameters, particularly focusing on sound absorption and sound reduction index, of the compressed CSL-WHA blocks. By identifying and understanding these acoustic properties, we can bridge the existing knowledge gap, paving the way for the development of construction materials that are not only cost-effective and eco-friendly but also proficient in meeting the essential acoustical standards, thus ensuring a comprehensive solution for sustainable construction practices.

1.3 Objectives of the study

1.3.1 General Objective

To comprehensively investigate the acoustical properties of compressed soil blocks with a binder mixture of lime and water hyacinth ash (CSL-WHA blocks).

1.3.2 Specific Objectives

i. To fabricate compressed earth blocks using a binder mixture of lime and water hyacinth ash, ensuring uniformity and structural integrity.
ii. To evaluate the acoustical properties of CSL-WHA blocks by recovering key parameters, porosity, through inverse modeling of transmission data.
iii. To assess how binder ratios (lime vs. WHA) influence acoustic properties of CSL- WHA blocks.
iv. To examine effect of compaction pressure on the acoustic properties of the blocks.

1.4 Research questions

i. How accurately does acoustic modeling retrieve the intrinsic acoustical parameters of CSL-WHA blocks?

ii. To what extent do CSL-WHA blocks meet established acoustical requirements for construction materials?"

iii. What is the impact of variations in compaction pressure on the acoustic behavior of CSL-WHA blocks?

1.5 Justification of the study

The imperatives of sustainable construction and the burgeoning environmental concerns associated with the construction industry highlight the critical need for innovative solutions. Compressed Soil Blocks (CSBs) stabilized by lime and WHA represent a significant stride in the direction of sustainable construction practices. However, optimizing their acoustic properties is a crucial frontier. By comprehensively understanding and enhancing the acoustical attributes of CSBs, we not only bolster energy efficiency but also foster environmentally friendly construction methodologies.

i. Advancing Energy Efficiency

A profound comprehension of the acoustic properties of CSBs equips us with the knowledge to enhance their energy efficiency. By optimizing sound absorption and sound reduction capabilities, these blocks can contribute to an environment that demands reduced energy consumption for climate control and create spaces characterized by acoustic comfort.

ii. Environmentally Friendly Construction

The study serves as a pivotal bridge between construction innovation and environmental preservation. By refining the acoustical properties of CSBs, we pave the way for construction practices that are not just eco-conscious but also technologically sophisticated. Such advancements align construction methodologies with the urgent global need for sustainable,

environmentally friendly practices.

i. Reduction in Greenhouse Gas Emissions

A holistic understanding of the acoustical nuances of CSBs offers a unique opportunity to reduce greenhouse gas emissions. By creating more efficient sound absorption materials, there is a direct impact on the demand for insulation, potentially leading to a decrease in the production and utilization of high-emission materials. This, in turn, aids in reducing the carbon footprint associated with traditional construction methods.

ii. Lowering Construction Costs

Beyond its environmental implications, optimizing the acoustic properties of CSBs has profound economic ramifications. Construction costs can be significantly lowered by developing materials that offer superior acoustic insulation, potentially reducing the need for additional soundproofing measures. This economic efficiency ensures that sustainable construction practices are not just environmentally viable but also financially practical.

iii. Mitigating the Impact of Water Hyacinth:

The study's findings extend beyond construction efficiency; they hold the potential to mitigate the environmental impact of water hyacinth. By harnessing this abundant yet challenging resource, we not only develop sustainable construction materials but also contribute to the mitigation of water hyacinth proliferation, addressing a pressing ecological concern at the same time.

iv. Enhancing Multi-Capable Materials:

The study contributes to the development of multi-capable materials crucial for modern construction demands. Acoustic optimization of CSBs enhances their versatility, making them invaluable in various construction scenarios. This adaptability is pivotal in addressing the diverse needs of contemporary architectural designs and construction projects.

In essence, this study is not merely an academic pursuit; it's a proactive step towards reshaping the future of construction. By delving into the intricate acoustical properties of CSBs, we forge a

path toward construction practices that are not only technologically advanced but also deeply considerate of the environment, paving the way for a sustainable and harmonious coexistence with our surroundings.

1.6 Significance of the study

The implications of this study extend far beyond the realms of construction; they resonate with crucial global concerns and have the potential to drive transformative change.

i. Environmental Impact and Greenhouse Gas Reduction:

The findings of this study stand as a beacon of hope in the battle against greenhouse gases. Cement production, notorious for its significant carbon dioxide emissions, can be mitigated through the adoption of CSL-WHA blocks. By justifying the replacement of cement with lime and WHA, this research paves the way for a significant reduction in CO_2 emissions, aligning construction practices with environmental preservation efforts.

ii. Energy Efficiency and Climate Control:

CSL-WHA blocks, with their low thermal conductivity, act as natural insulators, creating spaces that are naturally warmer in winter and cooler in summer. This intrinsic property reduces the energy demand for internal climate control systems. The study's insights not only contribute to energy efficiency but also promote sustainable living environments, fostering a balance between human comfort and ecological responsibility.

iii. Sustainable and Economic Construction Solutions

By showcasing the viability of construction blocks made from soil, lime, and WHA, this study offers a sustainable alternative. The abundant availability of soil, coupled with the energy-efficient production of lime and WHA, translates into economically friendly construction solutions. The study's outcomes empower the construction industry to embrace materials that are not only cost-effective but also environmentally sound, setting a new standard for sustainable building practices.

iv. Mitigating Water Hyacinth Challenges:

Water hyacinth, a persistent ecological problem, finds an unexpected solution in CSL-WHA blocks. By utilizing water hyacinth as a core component of construction materials, this study provides a tangible way to mitigate its multifaceted challenges. From preserving biodiversity to ensuring human and aquatic species' safety, the integration of water hyacinth in construction materials promises a holistic approach to reducing its adverse effects.

v. Resistance and Versatility

CSL-WHA blocks exhibit exceptional resistance. They are mold, insect, fire, and rodent-resistant, enhancing the longevity of constructions and reducing maintenance costs. Furthermore, their versatility allows them to be adapted to diverse architectural designs and construction needs, opening the door for innovative and resilient building solutions.

In essence, this study transcends the boundaries of conventional research. It emerges as a catalyst for a sustainable future, where construction practices are not just economically viable but also environmentally conscious. By addressing climate change, promoting energy efficiency, providing economical alternatives, and mitigating ecological challenges, the findings of this study usher in a new era of construction, one where harmony with nature is not just an ideal but a tangible reality.

1.7 Assumptions of the study

In delineating the scope of this study, several foundational assumptions are made to structure the research methodologies and analyses. These assumptions serve as essential guidelines while recognizing the complexities inherent in acoustical studies:

i. Material Homogeneity

The study assumes a consistent material composition within the specimens, considering CSL-WHA blocks as porous mediums. Acknowledging real-world material complexities, this assumption provides a fundamental framework for analysis, allowing for focused investigations into the acoustical behaviors of the porous structure.

ii. Constant Sound Intensity

The study operates under the premise of a consistent sound intensity throughout the experimentation, a necessary simplification for controlled analysis. While recognizing the dynamic nature of real-world sound scenarios, this assumption establishes a foundational baseline. Future research endeavors may explore nuanced variations in sound intensity, enhancing our understanding of diverse acoustic environments.

iii. Wave Propagation in Fluid and Porous Medium

The study considers wave propagation both in the fluid medium and within the porous structure of CSL-WHA blocks. The propagation model employed adopts an equivalent fluid medium approach, incorporating the Johnson-Champouc-Allard- Lafarge models to account for viscous and thermal effects. This assumption allows for in-depth exploration of acoustical interactions within the complex fluid-porous medium system, offering insights into the interplay of waves in diverse mediums.

By embracing these assumptions, the study navigates the intricate landscape of acoustical phenomena within porous mediums. However, it remains vital to critically assess these assumptions, encouraging ongoing research to refine models, incorporate real-world complexities, and deepen our understanding of acoustical behaviors in multifaceted environments.

1.8 Limitations of the study

In the pursuit of scientific rigor, this study recognizes several inherent limitations that shape the scope and interpretation of the research findings:

i. Low-Frequency Testing Accuracy

The waveguide's effective frequency range (18.8–2467.4 Hz) constrained data acquisition below 18.8 Hz, hence diminishing the precision of acoustic characterization in the low-frequency spectrum, particularly for viscous and thermal interactions. The effect of this constraint was decreased by the use of enhanced multi-taper spectral estimation to better resolve low-frequency behavior.

ii. Waveguide Vibrations

The study acknowledges the potential influence of vibrations within the waveguide structure. Whether stemming from external sources or internal mechanisms, these vibrations can introduce noise and distortions in the data. To minimize these effects, the experiment was carried out in a quiet environment to isolate external acoustic noise. In addition, a stiffer waveguide was used to help minimize self-noise.

iii. Boundary Conditions

The study operates within defined boundary conditions, essential for controlled experimentation. However, these boundaries inherently limit the applicability of the findings to specific contexts. Variations in real-world scenarios might introduce additional complexities not accounted for within the study's confined boundaries, necessitating cautious extrapolation of the results. To minimize this, a finite element acoustic model was used to simulate the acoustic environment.

iv. Signal degradation at high compaction pressures.

Highly compressed blocks produce weak acoustic signals, complicating the reliable retrieval of high-frequency parameters. This effect was minimized by the use of a highly sensitive microphone, applying a pre-amplification technique. The compaction regime was also adjusted to remain within optimal acoustic ranges for reliable parameter identification.

By transparently acknowledging these limitations, the study maintains scientific integrity and provides a foundation for future research. These constraints, while posing challenges, also serve as catalysts for innovative solutions, urging the scientific community to explore methodologies that surmount these limitations and expand the horizons of acoustical research.

1.9 Scope of the study

This study explored and analyzed the acoustic performance of compressed earth blocks made with a binder mixture of lime and water hyacinth ash (CSL-WHA blocks). The scope includes:

i. Development and Manufacturing: The study encompassed the creation of CSL-WHA blocks, focusing on achieving uniformity and structural integrity in the blocks through the use of a binder mixture of lime and water hyacinth ash.

ii. Evaluation of Acoustical Properties: The research involved a thorough evaluation of the acoustical properties of CSL-WHA blocks. Key characteristics such as porosity, tortuosity, viscous characteristic length, and airflow resistivity were assessed to understand the acoustic performance of the blocks.

iii. Binder Concentration Effects: The impact of varying concentrations of lime and water hyacinth ash on the acoustical properties was investigated.

iv. Compaction Pressure Analysis: The study analyzed the effects of different compaction pressures on the acoustic properties of CSL-WHA blocks.

Generally, the study provides insights into how the formulation and production parameters of CSL-WHA blocks influence their acoustic performance, contributing to the optimization of these blocks for construction applications.

CHAPTER TWO

LITERATURE REVIEW

2.1 Introduction

This chapter highlights various issues and research relevant to the study. It entails: water hyacinth ash as a pozzolanic material, lime as a binder in compressed soil blocks, acoustic damping and characterization of air-saturated materials, and the inverse identification of acoustic parameters.

2.2 Water Hyacinth as a pozzolanic material

The growing consciousness surrounding sustainable construction practices has spurred the adoption of environmentally and economically sound materials. This trend is driven not only by a desire to preserve natural resources but also by the imperative to mitigate the environmental impact of traditional construction materials such as cement. Cement production, notorious for its heavy consumption of natural resources and emission of toxic gases, is a significant contributor to global carbon dioxide emissions, accounting for approximately 7% of human-induced CO_2 emissions annually (Langaroudi & Mohammadi, 2018). In response, researchers are actively seeking alternative materials with pozzolanic properties to substitute for cement in concrete and soil block production, aiming to reduce the carbon footprint of construction activities.

Among these alternatives, water hyacinth ash (WHA) has attracted attention due to its abundance, low cost, and promising pozzolanic properties, characterized by high silica and calcium oxide content. Its potential to partially replace cement has been explored by Roychand et al. (2021), who demonstrated that WHA-enhanced concrete mixes offered improvements in environmental sustainability and reductions in embodied energy, paving the way for eco-friendly construction technologies.

Abana et al. (2021) delved into the potential of pulverized water hyacinth as an admixture for concrete, focusing on its impact on setting time and compressive strength. By manually pulverizing dried water hyacinth and incorporating it into concrete mixtures at varying percentages, they observed intriguing effects on both setting time and compressive strength. Notably, their

findings align with previous research indicating that WHA can alter the water absorption characteristics of concrete, thereby influencing setting time (Goel and Kalamdhad, 2018). Furthermore, the study revealed that the addition of pulverized WH can either accelerate or retard setting time depending on the concentration employed, underscoring the need for further investigation into optimal blending ratios. While these studies evaluate mechanical properties, they do not extend their scope to acoustic characterization, leaving a gap in understanding how binder concentration affects sound transmission and absorption, one of the core objectives of this study.

Similarly, studies by Murugesh and Balasundaran (2017) and Das and Singh (2016) have explored the use of WHA as a partial replacement for cement in concrete formulations. These investigations have highlighted the potential of WHA to enhance compressive strength while offering insights into its effects on workability and setting time. Additionally, Das and Singh (2016) conducted comprehensive analyses of WHA properties, including chemical composition, particle size, and water absorption, to assess its pozzolanic activity and compatibility with cementitious materials. Water absorption was calculated as a percentage of initial mass;

$$Water\ absorption\ (\%) = \frac{B-A}{A} \times 100, \tag{2.1}$$

where A is the dry weight of the mortars and B is the wet weight of the mortars taken having submerged them in water for twenty-four hours. In order to gauge the mortar cubes' capillary suction when they come into contact with water, sorptivity was used. An electronic balance was used to take masses every 120 minutes at a height of approximately 5 mm above the base of the cubes. The sorptivity coefficient was calculated from the equation:

$$\frac{Q}{A\rho} = S\sqrt{t} \tag{2.2}$$

where t is the elapsed time, A is the specimen's surface area through which water penetrated, S is its sorptivity coefficient, ρ is the density of water, and Q is the amount of water absorbed. Their

findings revealed that WHA reduces sorptivity and moisture ingress, enhancing resistance in aggressive environments. These features, lower water uptake and increased porosity, may also hold implications for acoustic damping. However, WHA's behavior in terms of sound transmission, particularly in porous media like compressed soil blocks, remains largely unexamined.

Moreover, existing literature focuses almost exclusively on WHA paired with cement. The combination of WHA and lime, which offers carbon neutrality and compatibility with natural soils, has not been explored in acoustic contexts. This thesis addresses that gap by developing compressed soil blocks stabilized with WHA-lime binders and recovering intrinsic acoustical parameters such as porosity, tortuosity, airflow resistivity, and characteristic lengths through inverse modeling.

Another critical dimension absent from previous work is the influence of compaction pressure on WHA-modified blocks. Since pore structure and density directly affect acoustic performance, evaluating compaction regimes is essential. This study examines how varying compaction pressure interacts with binder concentration to steer the microgeometry of the porous matrix and tailor sound transmission characteristics.

In summary, WHA stands out as a renewable binder with ecological and structural promise. Yet, its role in acoustically viable and sustainable construction remains underexplored, particularly when combined with lime and optimized through controlled compaction. This research, therefore, contributes new knowledge by characterizing the acoustical behavior of CSL-WHA blocks and guiding material design for low-carbon, sound-efficient housing.

2.3 Lime as a binder in compressed soil blocks (CSBs)

Lime has long served as an effective stabilizer in compressed soil blocks (CSBs), enhancing durability, plasticity control, and compressive strength. According to Bell (1996), lime initiates cation exchange with clay particles, neutralizing surface charges and causing flocculation—a process that binds soil minerals into larger aggregates. This transformation decreases plasticity, improves workability, and alters pore structures critical to both mechanical and acoustic behavior. Multiple studies have explored optimal lime concentrations across diverse soil profiles. Alavez-Ramirez et al. (2012) achieved 16.5 MPa compressive strength with 10% lime in sandy soils, while Guettala et al. (2002) reached up to 15 MPa in clay-sand mixtures. Raheem et al. (2010) and Akpokodje (1985) proposed ideal lime ranges from 6% to 12%, confirming lime's versatility across soil types. Bogas et al. (2018) further supported this concentration band for optimal long-term performance.

Hybrid formulations combining cement and lime have demonstrated structural advantages. Nagaraj et al. (2014) and Malkanthi et al. (2020) reported increased strength when lime (5– 10%) was partially replaced with cement (3–7%), surpassing minimum standards (SLS 1382) that neither binder alone could achieve. These results suggest a synergistic interaction where lime reinforces clay fractions and cement secures sandy matrices.

However, despite widespread investigation into compressive behavior, lime's influence on acoustical properties, especially in porous media, is sparsely documented. The chemical reactions it initiates (e.g. formation of calcium silicate and aluminate hydrates) affect pore connectivity and density, which are intimately tied to airflow resistivity, tortuosity, and sound

absorption. Yet no studies evaluate how lime concentration or compaction pressure alters these intrinsic acoustic parameters.

From an environmental standpoint, lime presents compelling advantages over cement. Its production yields less CO_2 (0.75 tonnes vs. cement's 0.99 per tonne) and requires lower energy

input (EuLA, 2019). Moreover, carbonation reactions with atmospheric CO_2 offer partial sequestration benefits, contributing to a more carbon-neutral lifecycle.

In summary, the existing studies focused almost entirely on mechanical outcomes, leaving lime's influence on acoustical properties and microstructure underexplored, especially when paired with WHA and subjected to varying compaction pressure. This thesis extends the conversation by investigating lime's pairing with WHA, a bio-based pozzolan with promising ecological credentials, and evaluating how compaction pressure steers microstructural acoustical behavior. By retrieving acoustic coefficients via inverse modeling, the study offers new insights into optimizing sustainable CSBs that are not only structurally sound but also acoustically efficient for low-energy, climate-responsive housing.

2.4 Acoustic energy attenuation and characterization of air-saturated materials

The propagation and attenuation of sound in porous materials are governed by complex interactions between the saturating fluid (usually air) and the solid frame of the medium. These interactions, primarily inertial, viscous, and thermal, occur over varying relaxation times depending on the frequency and temporal characteristics of the acoustic excitation (Johnson, Koplik, & Dashen, 1987). In high-frequency regimes, they are modeled using causal integro-differential operators that behave as fractional derivatives in the time domain (Fellah & Depollier, 2000), while in low-frequency domains, parameters such as tortuosity, viscous permeability, thermal permeability, and porosity dominate the response (Lafarge, 1993). Among these, porosity stands out as a key descriptor influencing all forms of energy dissipation and is central to understanding both acoustic and mechanical behavior in porous blocks.

To capture these properties, contemporary studies employ inverse modeling frameworks that recover acoustic parameters from experimental wave transmission data. A seminal example is Mansour et al. (2016), who characterized compressed earth blocks (CEBs) using guided low-frequency acoustic waves (60–6000 Hz) in a 22-meter waveguide. Their approach involved solving an inverse problem where the transmission coefficients recorded across samples were

compared against simulations using the Johnson-Champoux-Allard-Lafarge (JCAL) model—assuming the soil matrix behaved as a rigid frame. Retrieved parameters included porosity, airflow resistivity, tortuosity, and both viscous and thermal characteristic lengths.

Mansour et al.'s 2016 findings revealed that compaction pressure significantly influenced acoustic transmission, with higher pressure resulting in reduced porosity and increased airflow resistivity. However, at very high compaction levels, signal degradation occurred due to excessive material density and low permeability, leading to poor signal-to-noise ratios that made some acoustic parameters difficult to retrieve accurately. Their study was limited to cement-stabilized blocks and maintained fixed binder concentrations, offering minimal insight into binder variability or alternative stabilizers. Despite its methodological rigor, the study leaves several critical gaps that this thesis addresses. First, it does not consider eco-friendly binders like lime or water hyacinth ash (WHA), whose chemical and structural behaviors differ markedly from cement. Secondly, it fails to investigate how varying binder concentrations influence microstructure and acoustic attenuation. Lastly, while compaction pressure is treated as a variable, its interaction with binder type and content remains unexamined.

Building on Mansour et al.'s 2016 framework, this study applies equivalent fluid models to CSL-WHA blocks, investigating how binder ratios and compaction pressure jointly shape the acoustic transmission behavior of compressed blocks. Using custom inverse modeling algorithms developed in Julia, the transmission coefficient data are fitted against simulated outcomes to recover intrinsic parameters such as tortuosity, viscous characteristic length, and thermal permeability. By doing so, this thesis contributes new knowledge on how sustainable binder systems affect both the physical and acoustical viability of compressed earth blocks, enhancing their potential for climate-resilient, low-emission housing.

2.5 The inverse identification

Inverse identification refers to the process of matching experimental measurements, such as transmission coefficients, with the output of an acoustic model to recover intrinsic material

parameters. This approach is particularly effective for porous media, where direct measurement of certain properties is either destructive, complex, or unreliable. Following standards established by Bolton and Hong (2009), inverse characterization techniques typically employ impedance tubes or waveguides to extract acoustical properties from porous samples.

The Johnson–Champoux–Allard–Lafarge (JCAL) model provides a robust framework for characterizing air-saturated porous materials. It defines six key parameters: porosity (ϕ), airflow resistivity (σ), tortuosity ($\alpha\infty$), viscous characteristic length (Λ), thermal characteristic length (Λ'), and thermal permeability (k_0'). While porosity and resistivity can be measured directly, the remaining parameters are best retrieved through inverse modeling. Zielinski (2015) proposed a method using surface impedance measurements with varying air gaps, enabling simultaneous recovery of these parameters through optimization algorithms (Lafarge et al., 2018).

In this study, inverse identification was applied to Soil–Lime–WHA blocks, using an equivalent fluid model to simulate wave propagation in the porous medium. The assumption of a light saturating fluid (air) is valid given the open-pore structure of compressed soil blocks. Transmission coefficients were measured using an impedance tube, and the Julia programming language was employed to simulate the model and perform parameter optimization. The cost function, representing the discrepancy between measured and simulated transmission data, was minimized to extract the optimal values of the six acoustic parameters.

This approach allows for the non-destructive recovery of tortuosity, characteristic lengths, and permeability, which are critical for modeling sound absorption and transmission in sustainable construction materials. By applying this method to CSL-WHA blocks, the study extends existing inverse modeling frameworks to eco-friendly binders and explores how binder concentration and compaction pressure influence acoustic behavior, an area previously not addressed in the literature.

CHAPTER THREE

MATERIALS AND METHODS

3.1 Introduction

This chapter outlines the research design, testing methodology for analyzing the soil, processing of the WHA, mix proportions, production of test blocks, and acoustic characterization of the obtained blocks. It is a systematic series of procedures which ended up with the retrieval of the six-acoustic parameters ($\phi, \sigma, \alpha_\infty, \mathbf{\Lambda}, k', \mathbf{\Lambda}'$) from the measured transmission coefficient using an equivalent fluid material model of a porous CSL-WHA slab in an impedance tube. Because a light fluid is saturated in the porous compressed CSL-WHA blocks, the fluid model which is an approximation is justified in this case.

3.2 Research design

The study for potential use of a mixture of lime and WHA as a binder in the fabrication of CSBs was conducted systematically through a series of experiments as shown in figure 3.1.

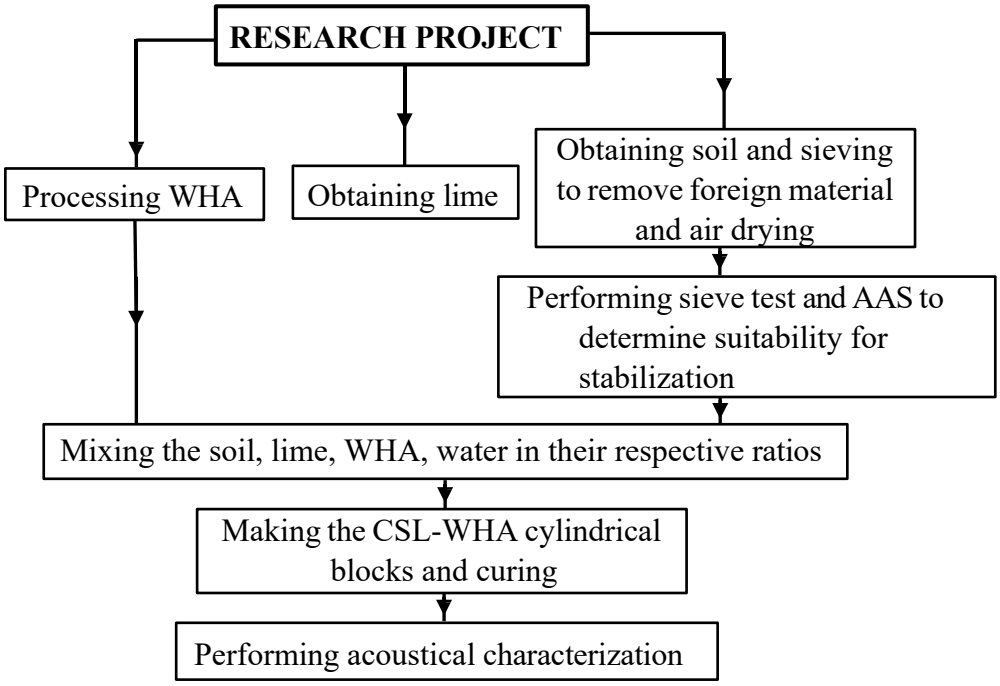


Figure 3.1: Research framework for fabrication and acoustic characterization of CSL-WHA

3.3 Raw materials

The materials used in making of the blocks are: natural site soil, lime, WHA and water.

The soil was obtained from Mayenje Ward, Matayos Sub- County in Busia County (Kenya) and then air-dried. A sieve test (ASTM D422-63, 2007) was performed on the soil sample in order to determine its grain size distribution. Using the information obtained from the sieve test, the soil was classified using the process provided by Unified Soil Classification System- USCS (ASTM D2487, 2000). A typical commercial class A lime that complies with the requirements of the specification (ASTM C110-20, 2020) was used as testing lime. The soil was further subjected to atomic absorption spectroscopy (AAS) to determine whether its elemental composition supports stabilization.

Water hyacinth (WH) used was collected from Dunga Beach (Kisumu) in Kisumu County. Fresh WH stems were thoroughly washed with clean water to get rid of debris and impurities, cut into 2-inch pieces using a sharp table knife and sundried for two weeks. The dried WH stem were thereafter incinerated in an incinerator at 800^0C for six hours in order to convert the organic matter into inorganic substance, and then ground using a laboratory scale ball mill for 30 minutes (Das & Singh, 2016). The ground WHA were finally passed through a 150-micron sieve as per IS: 1727-1967 to obtain the final WHA with fineness similar to that of OPC (Murugesh & Balasundaram, 2017).

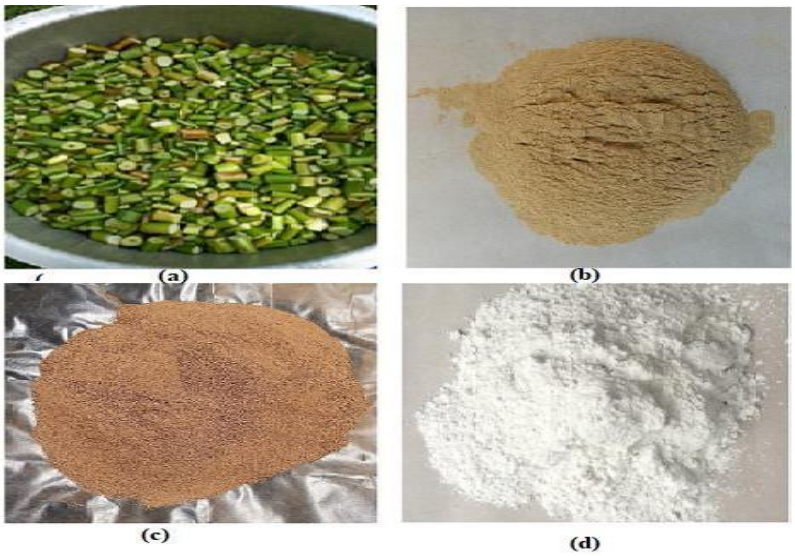


Figure 3.2: (a) Fresh cut WH stems (b) The final WHA, ready for use; (c) The final sieved soil, ready for use; and (d) The prepared lime

3.4 Mix-proportions for soil, lime, WHA and water

A total of 16 mixtures designated M-1 to M-16, were prepared for fabrication of the CSL-WHA blocks. The material proportions used in the design mixes were as in Table 3.1;

Table 3.1: Mix-proportions for soil, lime, WHA and water

Mix-designation	Pressure (Bars)	Constituent Material (% by mass)			Water (% mass of constituent material	Replicates
		Soil	Lime	WHA		
M-1	25	90	10	0	30	4
M-2	25	90	7	3	25	4
M-3	25	90	5	5	40	4
M-4	25	90	3	7	30	4
M-5	50	90	10	0	30	4
M-6	50	90	7	3	25	4
M-7	50	90	5	5	40	4
M-8	50	90	3	7	30	4
M-9	75	90	10	0	30	4
M-10	75	90	7	3	25	4
M-11	75	90	5	5	30	4
M-12	75	90	3	7	30	4
M-13	100	90	10	0	25	4
M-14	100	90	7	3	40	4
M-15	100	90	5	5	30	4
M-16	100	90	3	7	30	4

Blocks with 10% lime and 0% WHA served as the control mix. This allowed benchmarking on how WHA additions affected acoustic transmission and microstructure. Studies have shown that 10% lime yields optimal mechanical performance across soil types (Bogas et al., 2018; Guettala et al., 2002) and that mixes above 10% reduce workability (Nagaraj et al., 2014).

The use of 90% soil was a strategic choice rooted in sustainability, structural adequacy, and acoustic enhancement. Soil serves as the primary matrix, offering low embodied energy and local availability. The 90:10 ratio of soil to binder ensures optimal material synergy, balancing mechanical performance with eco-efficiency, as supported by studies such as Alavez-Ramirez *et al.* (2012) and Nagaraj et al. (2014), which confirm that low lime content can yield durable, sustainable construction materials.

3.5 Preparation of the CSL-WHA blocks

The soil was sieved through an 8 mm aperture size sieve prior to the manufacture of the CSBs so as to retain particles whose sizes were less than 8 mm. The sieved soil was then oven-heated at 105 ^{0}C for 24 hours. The dried soil was then mechanically mixed with lime and WHA in various designated ratios, after which water was added and the mixing continued until the mixture became homogeneous (Mansour et. al., 2016). The volume of water added was determined using the drop test (Ipinge,2012).

The mixture was then compacted in a cylindrical mold of internal diameter 76mm so that it just fits exactly across the cross-section of the waveguide and a height of 20mm for them to be easily characterized in a low frequency regime. The pressing was done using a hydraulic press (Hydraform, model number M7TWIND, South Africa). Four replicates for each mix proportion designated M-1 to M-16 were made (Table 3.1). After compaction, the CSL-WHA blocks were cured for a period of 28 days under plastic sheeting for them to gain adequate mechanical strength for use in acoustic characterization. Figure 3.3c shows the prepared CSL-WHA samples.

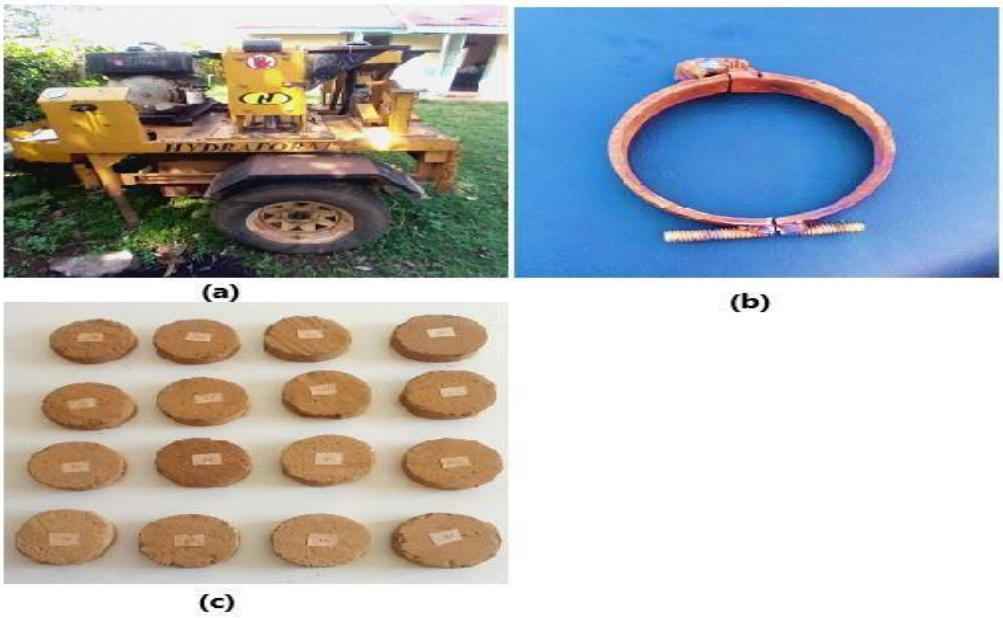


Figure 3.3: (a) Mobile hydra-form block making machine (image taken at Busia County, department of housing); (b) Fabricated cylindrical mould for making CSL-WHA sample slabs; (c) The prepared CSL-WHA sample slabs for tests.

3.6 Acoustic characterization of the CSL-WHA block

The measurement of the acoustic transmission coefficient was performed using a waveguide of length 18 m and an internal diameter of 0.076 m. The cylindrical CSB-WHA samples made to fit exactly into the cross-section of the waveguide were inserted 3 m downstream of the acoustic source, one at a time. The edges of the samples were sealed using a black tape. An omnidirectional microphone with an integrated preamplifier was placed 12 m downstream of the pipe from the acoustic source (9 m from the CSB-WHA sample) in order to capture both the incident and the transmitted signals. The useful frequency range of the waveguide was 18.8 - 2,467.4 Hz, which was calculated according to the formula (Ogam, et. al, 2021):

$$f_L = \frac{v}{l+1.6r}; \quad f_H = \frac{1.8412v}{2\pi r} \qquad 3.1$$

where v is the speed of sound in the fluid (air in this case, which was taken as 320 m/s), l is the length of the pipe, r is the radius of the pipe, f_L is the low cut-off frequency of the waveguide and f_H is the high cut-off frequency of the waveguide. A transient sound wave was then

generated in the waveguide by a ribbon loud speaker (VIAWAVE SRT-7, SN 32237, Petrozavodsk, Russia), which was in turn connected to a signal generator (Thurlby Thandar TG 210 function generator, Huntingdon. Cambs UK). The generator was programmed to produce a Heaviside signal (step function). The acoustic leakage between the edges of the samples and the pipe walls due to the sample not being perfectly circular was prevented using putty (brand and address). The incident signal was captured before inserting the specimen (sample CSL-WHA blocks), while the transmitted signal was captured with the specimen fitted into the waveguide. The response signals obtained was then digitized using a digital storage oscilloscope from pico technology (picoscope 4262, United Kingdom), with a maximum frequency of 5 MHz and a bit rate of 16 bits, connected to the microphone (Figure 3.4).

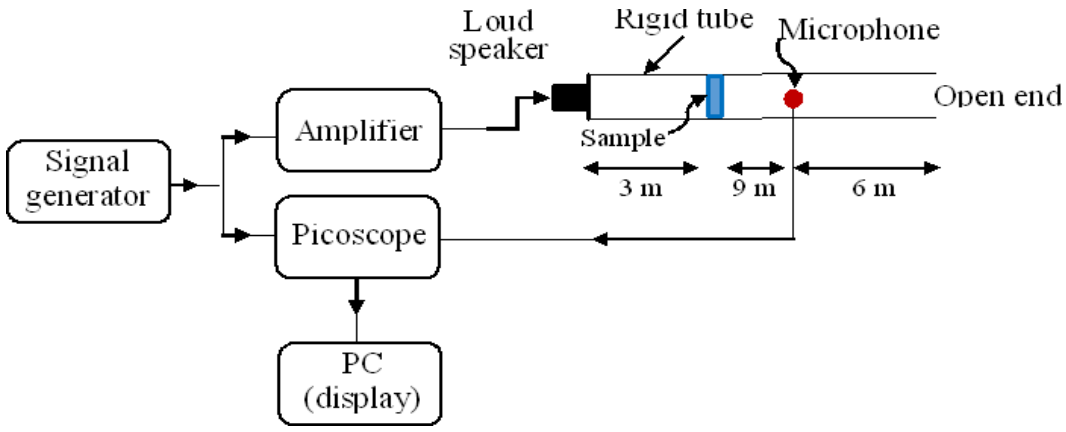


Figure 3.4: The experimental set up for the acoustic measurement of transmission coefficient of the samples

Exploitation of the data and simulation of the model was realized using the Julia programming language (Bezanson, Karpinski, Shah, and Edelman (2012). The transmission coefficient was obtained through the computation of the transfer function between the incident and transmitted signals. The transfer function $T_{IT}(f)$ is computed from the quotient of cross power spectral density S_{IT} of the incident $(P_I(t))$ and transmitted $(P_T(t))$ acoustic pressure and the power spectral density (S_{II} of $P_I(t)$) (Ogam, Fellah, Ongwen and Oduor, 2021):

$$T_{IT}(f) = \frac{S_{IT}(f)}{S_{II}(f)} \qquad 3.2$$

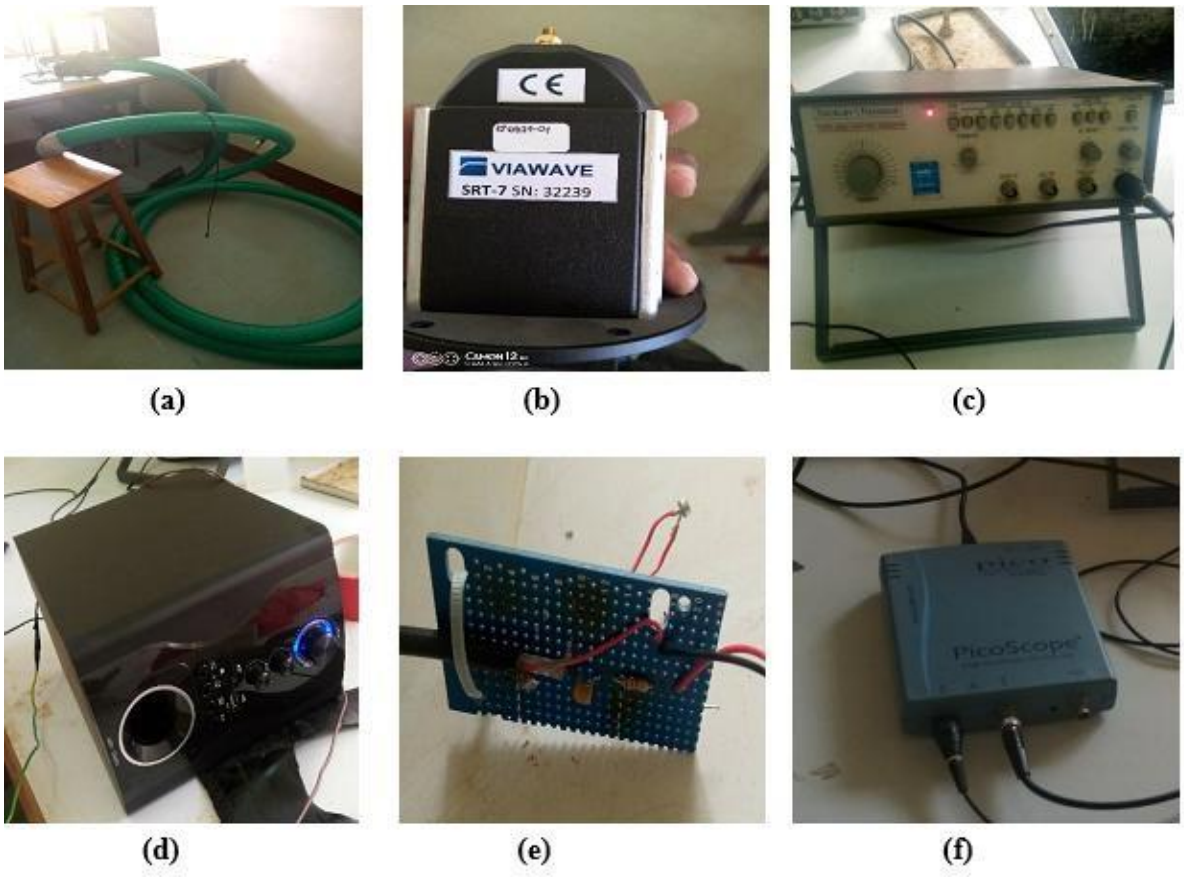


Figure 3.5: (a) Coiled waveguide (b) Ribbon loud speaker (c) Signal generator (d) Sub-woofer (e) Omnidirectional microphone (f) Pico scope

3.7 Solution of the inverse problem for the determination of acoustical parameters

The analytical expression of the transmission coefficient for a porous rigid frame plate of infinite dimensions in the frequency domain considered in this work was derived from an earlier study by Mansour et al. (2016) from the wave propagation equation. The equation is given by:

$$\mathrm{T}^{\mathrm{EFM}}(\omega) = \frac{2\phi \mathrm{x_r}}{\mathrm{j}(\mathrm{x_r^2}+\phi^2)\sin(k_1 \mathrm{d}) + 2\mathrm{x_r}\phi\cos(k_1 \mathrm{d})}, \qquad 3.3$$

where $\mathrm{T}^{\mathrm{EFM}}$ is the equivalent fluid model (EFM) transmission coefficient, $\mathrm{K_f} = \omega/\mathrm{c_f}$ is the wavenumber and $\mathrm{c_f}$ is the wave velocity in the fluid, k_1 is the wave number in the porous layer $\left(k_1(\omega) = \omega\sqrt{\frac{\rho_f \alpha(\omega)\gamma(\omega)}{\mathrm{K_f}}}\right)$, $\mathrm{x_c} = \rho_1 c_1$ is the characteristic specific acoustic impedance of the

porous medium (c_1 is the wave velocity), $x_f = \rho_f c_f$ is that of free air, $x_r = x_c/x_f$ is their ratio, and d = △L is the thickness.

The coefficient α(ω)γ(ω) is the refractive index of the medium that changes the wave velocity from $c_f = \left(\frac{\rho_f}{K_f}\right)^{-\frac{1}{2}}$ in free space to $c_1(\omega) = \frac{c_f}{\sqrt{\alpha(\omega)\gamma(\omega)}}$ in the porous medium.

The frame models of the dynamic tortuosity by Johnson, Koplik and Dashen (1987), and the dynamic compressibility modeled by Champoux and Allard (1991), and later improved by Lafarge (1993) were chosen because they provide a complete description of the inertial, viscous, and thermal interactions in the porous soil blocks. They are the dynamic tortuosity (α(ω)) and the dynamic compressibility, modify respectively the fluid density (ρ_f) and the fluid compressibility (K_f) through the multiplier process to obtain the modified parameters of the porous medium in the frequency domain ($\rho_1 = \rho_f\alpha(\omega)$ and $K_1 = K_f\gamma(\omega)^{-1}$).

$$\alpha(\omega) = \alpha_\infty \left(1 + \frac{\lambda\phi}{j\omega\alpha_\infty\rho_f k_0}\sqrt{1 + j\frac{4\alpha_\infty^2 k_0^2\rho_f\omega}{\lambda\Lambda^2\phi^2}}\right) \quad 3.4$$

$$\gamma(\omega) = \vartheta - (1-\vartheta)\,x\left(1 + \frac{\lambda\phi}{j\omega\rho_f k_0' P_r}\sqrt{1 + j\frac{4k_0'^2\rho_f\omega P_r}{\lambda\Lambda'^2\phi^2}}\right), \quad 3.5$$

with $j = \sqrt{-1}$, λ is the viscosity, ϕ and α_∞ are respectively, the porosity and tortuosity of the porous medium, Λ and Λ′ are the viscous and thermal characteristic lengths, ρ_f , is the density of the fluid, P_r is the Prandtl number. The static viscous permeability ($k_0 = \lambda/\sigma$) is an intrinsic parameter that depends only on the geometry of the pores (σ is the airflow resistivity). k_0' is the static thermal permeability (Lafarge, Lemarinier, Allard and Tarnow, 1997), which partly characterizes the thermal effects at low frequencies.

The inverse problem (IP) of an acoustic wave transmission by a porous material in this study involved the retrieval of the six acoustic wave parameters (ϕ, σ, Λ, $\propto_\infty$, Λ'/Λ and k_0') from the measured transmission coefficient of a porous slab in a long pipe and an acoustic/CSB interaction model of wave transmission using an EFM. An error functional that expresses the difference between the

transmission coefficient data and the interaction model, and from the experiment was computed for each set of trial values of the six microgeometry and transport acoustical parameters. Choosing the functional Ƒ that expresses this discrepancy was:

$$Ƒ(\omega, \phi, \sigma, \Lambda, \propto_{\infty}, \Lambda'/\Lambda, k_0') = \sum_{n=1}^{N}\left(\left|T^{EFM}(\omega, \phi, \sigma, \Lambda, \propto_{\infty}, \Lambda'/\Lambda, k_0')\right| - \left|T_{IT}^{exp}(\omega)\right|\right)^2 \quad 3.6$$

Here, T_{IT}^{exp} denotes the transmission coefficient obtained from the experimental data. The objective function Ƒ enables the optimization of model parameters to minimize the difference between predicted and measured values, leading to more accurate and reliable acoustic analysis and design. Through minimization of the objective function Ƒ, the six acoustical parameters were retrieved. The minima were found through varying the acoustical model parameters at small intervals (Wirgin, 2016): ϕ was varied at interval of 0.01, σ at 200, Λ at 2.0 x 10^{-6}, $\propto_{\infty}$ at 0.01, Λ'/Λ at 0.01, and k_0' at 1.0 x 10^{-10}. The solutions of the acoustical parameters were obtained at the global minima of the cost functions against the respective acoustical parameters (Lefeuve-Mesgouez et al., 2013). The process was done for each parameter at a time (since it is manual), while keeping the others fixed (Mansour et al., 2016).

CHAPTER FOUR
RESULTS AND DISCUSSIONS

4.1 Introduction

In Chapter four, a comprehensive summary of the study's results is presented, highlighting key findings and providing insightful analyses to elucidate the observed outcomes.

4.2 Characteristics of soils used

4.2.1 Granulometric analysis

According to ASTM D422-63, Table 4.1 presents the findings of the granulometric analysis used to ascertain the breakdown of soil particle dispersion by diameter classes.

Table 4.1: Granulometry

Property	Characteristic	Value (Percentage)
Granulometry	Gravel (>4.75mm)	1.01
	Sand (4.75-0.075mm)	39.11
	Silt and clay (<0.075)	59.88

More than half of the soil sample from **Table 4.1** passed the No. 200 sieve (0.075mm openings). As a result, the soil is categorized as fine-grained soil, somewhat moderately plastic silt soil (Group A-4) by the Unified Soil Classification System-USCS (ASTM D2487, 2000) and the AASHTO (AASHTO, 2012) soil classification system.

It has been discovered that lime reacts well with medium, moderately fine, and fine-grained soils, reducing their plasticity and potential to swell while increasing their workability and strength. Moreover, AASHTO classifications indicate that soil types A-4, A-5, A-6, A-7, and portions of A-2-6 and A-2-7 are suitable for lime stabilization (Terrei, et al, 1979). Thus, lime and WHA work well as binders in the soil used in this study.

4.2.2 Atomic Absorption Spectroscopy

The elemental composition of the soil sample determined using AAS is summarized in Table 4.2

Table 4.2: Elemental composition of soil

Analysed parameters	Parameter values
Ph (1:2.5) Soil:Water	4.61
C.E.C (meg/100g)	5.90
Alluminium (ppm)	19
Phosphorus (%)	19.82
Potassium (meg %)	0.12
Aluminium oxide (ppm)	1.8
Calcium (meg %)	1.53
Magnesium (meg %)	2.42
Copper (ppm)	1.68
Iron (ppm)	10.40
Zinc (ppm)	5.44
Silicon dioxide (%)	15
Monosilic acid (ppm)	27

The elemental analysis of the soil sample used in fabrication of CSL-WHA blocks revealed a moderately acidic pH of 4.61, with a cation exchange capacity (CEC) of 5.90 meg/100g, indicating moderate reactivity and potential for stabilization. Silicon dioxide content measured at 15% and complimented by 27ppm of monosilic acid suggest a promising pozzolanic potential essential for binder formation and long-term strength development of the fabricated block. The presence of sufficient calcium (1.53 meg%) and magnesium (2.42 meg%) levels supports cementitious reactions (Mohankumar & Rakaraddy, 2018, Aquaaid, 2021), while trace elements such as iron (10.40 ppm), aluminium (19 ppm), and aluminium oxide (1.8 ppm) influence hydration kinetics and thermal conductivity (Adamczyk, 2015). This mineralogical profile supports the development of compressed soil blocks from this soil.

4.3 Effect of WHA and lime concentrations on the acoustic transmission coefficient

The change in the transmission coefficients of the CSL-WHA blocks (samples M-1 to M-4) with the variation in WHA and lime are shown in Figure 4.1, all prepared at a compaction pressure of 25 bars. This pressure allows clearer observation of how WHA and lime ratios influence transmission coefficients, without the confounding effects of excessive densification.

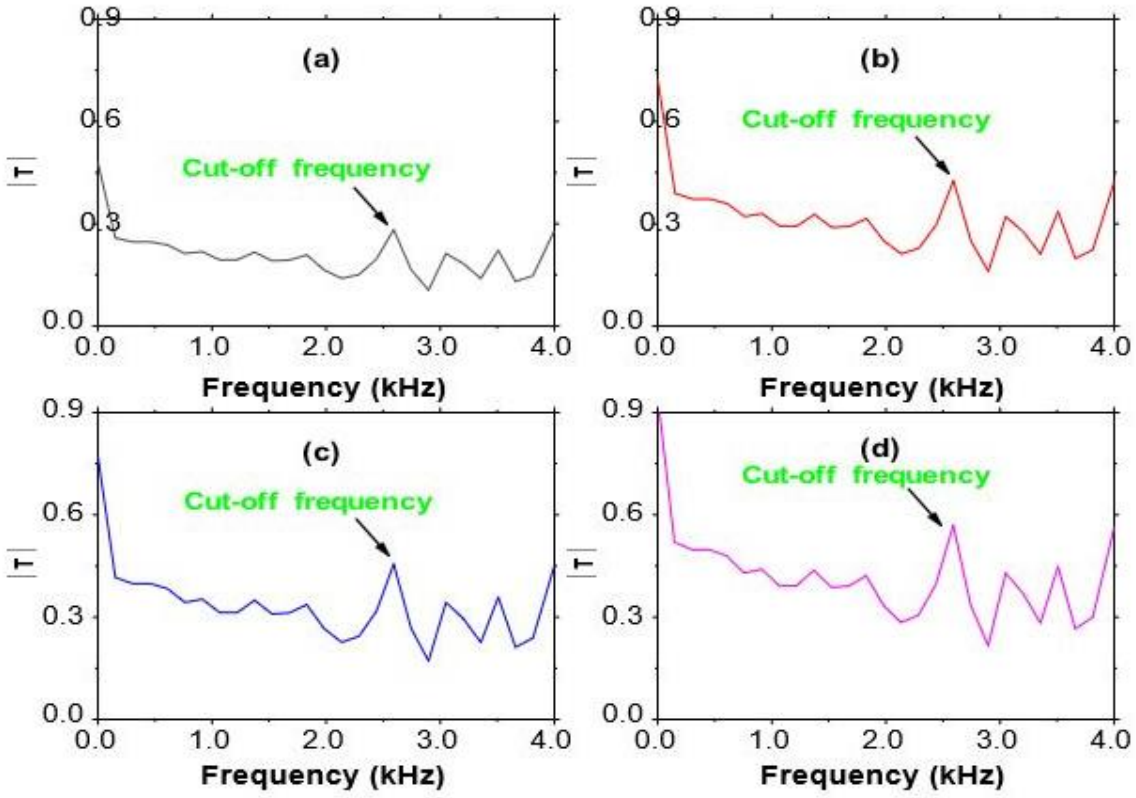


Figure 4.1: Transmission coefficient of the CSL-WHA samples at a pressure of 25 bars, with the soil at 90%. (a) 10% lime and 0% WHA; (b) 7% lime and 3% WHA; (c) 5% lime and 5% WHA; and (d) 3% lime and 7% WHA

Figure 4.1 illustrates an increase in the transmission coefficient as the percentage of WHA content rises across all mix designs M1 to M4, indicating an effect on porosity. This increase is visible in the progressively higher amplitude curves for each mix. As WHA content increases from 0% in M1 to 7% in M4, the transmission coefficient curves shift upwards, especially in the low to mid-frequency range (below 2500 Hz), where plane wave propagation dominates.

However, it is important to note that this observation alone does not reveal which specific

parameters are changing. The identification of these parameters will be covered in the next section through solving the inverse problem, enabling us to retrieve and analyse the factors influencing the observed rise in transmission coefficient.

The curves exhibit linear behaviour up to the cut-off frequency, but beyond this point, oscillations emerge. A distinct peak is noticeable around 2500 Hz, closely aligning with the theoretical upper cut-off frequency of the waveguide (2467.4 Hz). Beyond 2500 Hz, the wave nature shifts from plane waves to transverse modes within the circular cross-section waveguide. This shift signifies that above the cut-off frequency, the system can no longer support simple, undistorted plane waves, and instead, transverse modes manifest, introducing a more intricate wave behaviour. Consequently, the effective bandwidth is limited from 18.8 to 2500 Hz. Additionally, Figure 4.1 illustrates that as the frequency approaches 0 Hz, the transmission coefficient asymptotically approaches 1. Understanding the behaviour beyond the cut-off frequency is crucial for characterizing the waveguide's performance and assessing the range of frequencies over which it can efficiently transmit signals.

When lime is added to soil, the soil properties change. There is a consistent increase in the transmission coefficient with reduction in the lime content. When lime is added to the soil water system, hydroxide (OH^-) and calcium (Ca^{2+}) ions are produced. Bivalent Ca^{2+} ions are swapped out for monovalent cations in cation exchange. By forming a bond between the minerals in the soil, the Ca^{2+} ions lessen the repulsion forces and the thickness of the diffused water layer. The soil particles are encased in this layer, which strengthens their relationship. The elevated alkalinity in the solution is caused by the residual anions (Mallela et al., 2004; Geiman, 2005). The texture of the soil changes as a result of the soil particles grouping into large sizes (Terrei et al., 1984). The process of flocculation-agglomeration leads to the creation of floc. The void ratio rises as a result of the larger particle size (Kinuthia et al., 1999).

The rise in the void ratio results in an increase in the transmission coefficient. However, at higher

quantities of lime in soil, the pH of the soil increases above 10.5 resulting in the release of silica and alumina in the soil. The silica and alumina components of the soil react with the calcium from the lime to form calcium silicate hydrates (CSH) and calcium aluminate hydrates (CAH) respectively.

$$Ca(OH)_2 + SiO_2 \longrightarrow CaO\text{-}SiO_2\text{-}H_2O \quad (4.1)$$

$$Ca(OH)_2 + Al_2O_3 \longrightarrow CaO\text{-}Al_2O_3\text{-}H_2O \quad (4.2)$$

The cementitious minerals, CSH and CAH, alter the stabilized soil's micropore structure. The soil is altered from sandy granular material to hard relatively impermeable layer. This explains why the CSL-WHA blocks at 10% lime have the lowest transmission coefficient from which it increases as the concentration of lime decreases.

Addition of WHA in the blocks manufacturing process causes the granular packing and fluid phases of the block to realign by increasing the number of microscopic and macroscopic holes. This increases the void ratio hence higher transmission coefficient than that of lime alone. The WHA does not significantly increase the alkalinity of the soil hence minimal release of silica and alumina in the soil. Therefore, as more lime is replaced with WHA, there is significant decrease in formation of CSH and CAH rendering the CSL-WHA blocks more permeable. This explains why the transmission coefficient increases as the WHA ratio increases. WHA is a good source of magnesium oxide which research has shown that is more stable and more resistant to sulphate attack. Blending WHA with lime reduces pulverization since it results in the formation of magnesium carbonate in addition to calcium carbonate, considered a stronger bond than calcium carbonate alone, and improves pozzolanic reactions (Mo and Panesar, 2012; Panesar and Mo, 2013).

4.4 The intrinsic acoustic parameters of the CSL-WHA blocks

These parameters are not directly measurable hence they were obtained by solving an inverse problem based on transmission coefficient data, following the approach outlined by Mansour et al. (2016). Experimentally measured transmission coefficients were compared with those

predicted by the theoretical model and the discrepancy quantified using cost functions. By iteratively adjusting the input parameters to minimize these cost functions, an optimal set of non-acoustical properties was recovered.

Figure 4.2 presents the plots of the cost functions against each of the sought-for parameters (porosity, airflow resistivity, tortuosity, viscous characteristic length, thermal characteristic length, the ratio between viscous and thermal characteristic lengths, and thermal permeability) for sample M-4, selected as a representative case.

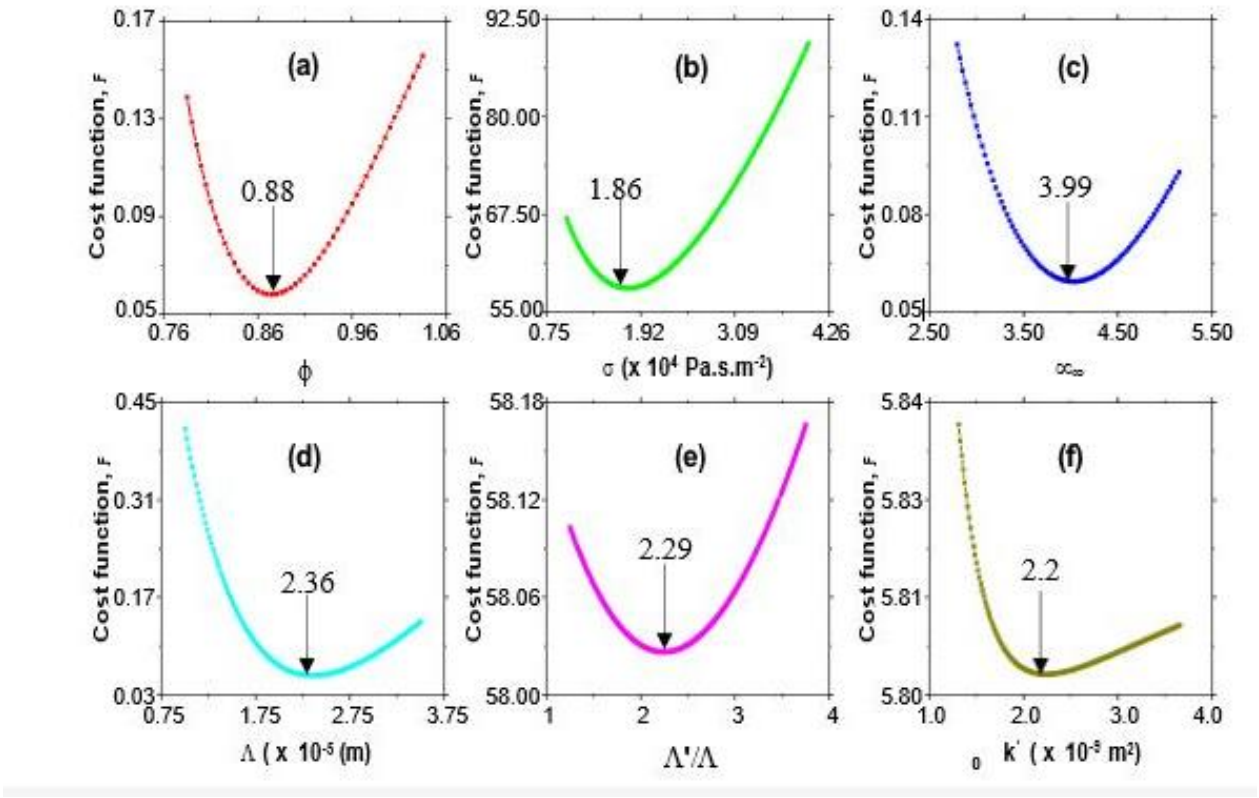


Figure 4.2: Plots of cost functional Ƒ against the sought-for acoustical parameters for sample M-4: (a) Porosity (ϕ), (b) Airflow resistivity (σ), (c) Tortuosity (α_∞), (d) Viscous characteristic length (Λ), (e) ratio (Λ'/Λ), and (f) thermal permeability (k_0').

The values of the sought-for parameters were obtained from the minima of the curves. As can be observed, unique minima around the intervals of the solutions were obtained for all the six sought for parameters.

After resolving an inverse acoustic problem, the intrinsic macroscopic acoustic characteristics (ϕ, σ, Λ, α) of the examined sample blocks were tabulated as shown in Table 4.2.

Table 4.3: Values of the parameters obtained using IP for the CSL-WHA sample blocks at various densities

Sample	Pressure (Bars)	$\boldsymbol{\rho(kgm^{-3})}$	∅	$\boldsymbol{\sigma(Pam^{-2}s)}$	$\boldsymbol{\alpha}$	$\boldsymbol{\Lambda(m)}$	$\boldsymbol{\Lambda/\Lambda'}$	$\boldsymbol{k_o}$
M1	25	2202	0.52	89400	1.68	0.0000098	2	9.3E- 10
M2	25	1857	0.64	45400	2.74	0.0000182	1.93	1.6E-09
M3	25	1787	0.78	35600	3.38	0.0000244	1.89	7.9E-09
M4	25	1615	0.88	18600	3.99	0.0000236	2.29	2.7E-09
M5	50	2259	0.35	106000	1.58	0.0000114	1.87	2.2E-09
M6	50	2041	0.38	55400	1.8	0.0000228	1.83	8E-10
M7	50	1913	0.51	48200	1.79	0.0000168	1.89	6.5E-09
M8	50	1885	0.57	28800	2.06	0.000025	1.89	6.4E-09
M9	75	2308	0.31	133600	1.45	0.00001	1.87	3.3E-10
M10	75	2168	0.36	71600	1.66	0.0000168	1.87	5.2E-09
M11	75	1961	0.42	65200	1.79	0.0000164	1.91	2.9E-09
M12	75	2004	0.47	42200	2.06	0.0000238	2.07	3.6E-09
M13	100	2536	0.25	183500	1.93	0.000015	1.9	1.3E-09
M14	100	2221	0.34	108800	1.97	0.0000146	1.88	6.4E-09
M15	100	2203	0.42	102600	2.24	0.000014	1.88	3.8E-09

4.5 Effect of concentration of WHA and lime on intrinsic acoustical properties

From the minima of the cost function curves, Figure 4.3 was obtained through plotting of the retrieved values of the macroscopic parameters describing the microstructure i.e., the intrinsic acoustical parameters of the blocks compacted at a pressure of 25 bars for samples M-1 to M- 4 (0–7 % WHA).

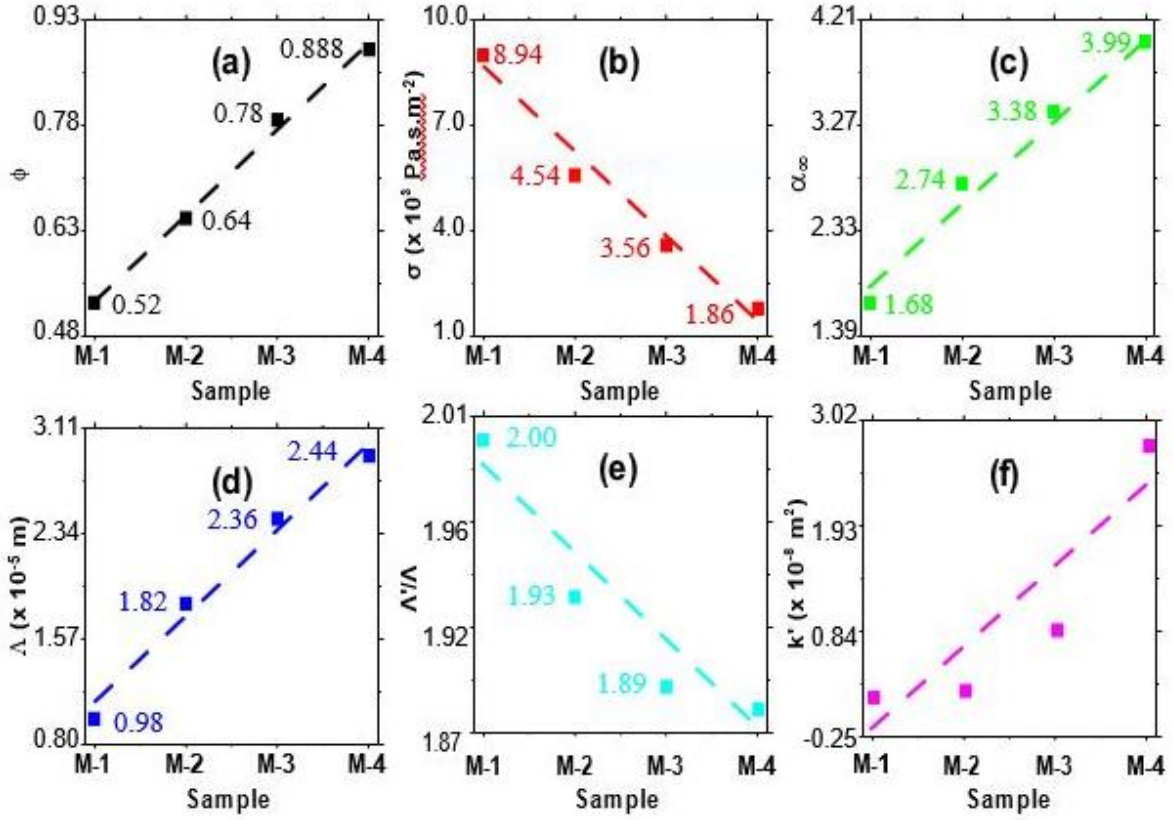


Figure 4.3: Plots of the intrinsic acoustical parameters: (a) porosity, ϕ; (b) airflow resistivity σ; (c) tortuosity α_∞; (d) viscous characteristic length (e) the ratio between thermal characteristic length Λ' and viscous characteristic length Λ; (f) thermal permeability (k_0') against the sample number (from M-1 to M-4), all at a compaction pressure of 25 bars.

4.5.1 Porosity

Porosity in CSL-WHA blocks increases with rising concentration of Water Hyacinth Ash (WHA) and decreasing lime content. As observed in Figure 4.3(a) and supported by Table 4.3, blocks transition from 0.52 porosity at 10% lime and 0% WHA (sample M-1) to 0.88 porosity at 3% lime and 7% WHA (sample M-4), under constant compaction pressure. Lime promotes formation of calcium silicate hydrates (CSH) and calcium aluminate hydrates (CAH), which densify the microstructure by filling pore spaces, thereby lowering porosity. In contrast, WHA disrupts particle packing and contributes to a more open structure with increased void spaces, amplifying porosity. Thus, higher WHA concentrations favour acoustic transmission by enhancing porosity, while greater lime content tends to tighten the matrix and reduce pore accessibility.

4.5.2 Air flow resistivity

Airflow resistivity in CSL-WHA blocks decreases as Water Hyacinth Ash (WHA) concentration increases and lime content decreases, a trend clearly illustrated in Figure 4.3(b) and supported by Table 4.3. At a constant compaction pressure of 25 bars, resistivity drops from 89,400 Pa·s/m² in sample M-1 (10% lime, 0% WHA) to 18,600 Pa·s/m² in sample M-4 (3% lime, 7% WHA). This decline reflects the shift in binder chemistry: lime promotes the formation of dense hydration products like calcium silicate hydrates (CSH) and calcium aluminate hydrates (CAH), which fill pore spaces and restrict airflow. WHA, being less reactive and more fibrous, disrupts granular packing and encourages the development of larger, interconnected pores. As lime is progressively replaced by WHA, the pore network becomes more permeable, allowing air to pass through more easily. Figure 4.3(b) visually confirms this trend, showing a consistent downward slope in resistivity values as WHA content increases across samples M-1 to M-4. This enhanced permeability contributes to improved acoustic transmission, supporting the use of WHA-lime blends in sustainable, sound-responsive construction.

4.5.3 Tortuosity

Tortuosity in CSL-WHA blocks increases as Water Hyacinth Ash (WHA) concentration rises and lime content decreases, a trend clearly illustrated in Figure 4.3(c) and supported by Table 4.3. At 25 bars compaction pressure, tortuosity values climb from 1.68 in sample M-1 (10% lime, 0% WHA) to 3.99 in sample M-4 (3% lime, 7% WHA). This parameter reflects the complexity of airflow paths through the porous structure. Higher tortuosity means air must navigate more winding, indirect routes. Lime contributes to a denser matrix by forming calcium silicate and aluminate hydrates (CSH and CAH), which streamline the pore network and reduce tortuosity. In contrast, WHA disrupts particle alignment and fosters irregular, elongated voids, forcing air to take more circuitous paths. As WHA replaces lime, the pore geometry becomes increasingly intricate, resulting in higher tortuosity. This shift enhances acoustic scattering and energy dissipation, making WHA-rich blocks more effective for sound absorption in sustainable construction.

4.5.4 Viscous characteristic length

Viscous characteristic length ($\boldsymbol{\Lambda}$) in CSL-WHA blocks quantifies how air interacts with the pore walls during sound propagation, especially at medium and high frequencies. From Figure 4.3(d) and Table 4.3, we observe a clear upward trend in $\boldsymbol{\Lambda}$ as Water Hyacinth Ash (WHA) concentration increases and lime content decreases. At 25 bars compaction pressure, $\boldsymbol{\Lambda}$ rises from 9.8×10^{-6} m in sample M-1 (10% lime, 0% WHA) to 23.6×10^{-6} m in sample M-4 (3% lime, 7% WHA). This increase reflects a shift in pore geometry: lime promotes the formation of dense hydration products (CSH and CAH), which narrow the voids and reduce the effective viscous interaction zone. WHA, being less reactive, disrupts this densification and encourages the development of wider, more irregular pores. As lime is replaced by WHA, the average pore size expands, allowing air to interact over a larger surface area hence the longer viscous characteristic length. This parameter directly influences acoustic attenuation and energy dissipation, making WHA-rich blocks more effective for sound absorption in sustainable construction.

4.5.5 Static thermal permeability

Static thermal permeability (k'_0) in CSL-WHA blocks exhibits a marked increase with rising Water Hyacinth Ash (WHA) concentrations and decreasing lime content—a pattern clearly displayed in Figure 4.3(f) and reinforced by values in Table 4.3. At 25 bars compaction pressure, k'_0 climbs from 9.3×10^{-10} m² in sample M-1 (10% lime, 0% WHA) to 2.2×10^{9} m² in M-4 (3% lime, 7% WHA). This shift reflects the evolving pore network: lime, through the formation of CSH and CAH compounds, densifies the matrix and hinders heat exchange by narrowing void channels. WHA, being less cementitious and more organic in texture, disrupts this packing and promotes larger, more continuous pores that facilitate thermal conduction. This increase in k'_0 corresponds to a more open and thermally accessible pore structure, where heat can transfer more efficiently between the solid frame and air-filled voids. As WHA increasingly replaces lime, the matrix evolves into a looser, more conductive architecture, optimizing both low-frequency sound damping and passive thermal regulation for energy- conscious construction.

4.6 Effect of compaction pressure on the transmission coefficient

The increase in compaction pressure exhibited a notable inverse relationship with the transmission coefficient, showcasing a decrease in transmission as pressure rose. This phenomenon can be attributed to the heightened compaction pressure causing a reorganization of the granular packing within the blocks and a rearrangement of fluid phases. Consequently, there is a reduction in the number of macroscopic pores, leading to a consequential decline in the magnitude of the transmission coefficient. This observed trend aligns with findings reported by Mansour et al. (2016), underlining the consistency of the impact of compaction pressure on the transmission properties of the soil blocks. Moreover, the influence of compaction pressure extends beyond its effects on transmission, playing a crucial role in shaping the overall structural and acoustical characteristics of the compressed soil blocks.

Figure 4.4 shows the variation of the transmission coefficient of samples M-2, M-6, M-10, and M-14 with frequency (all samples at the same concentration).

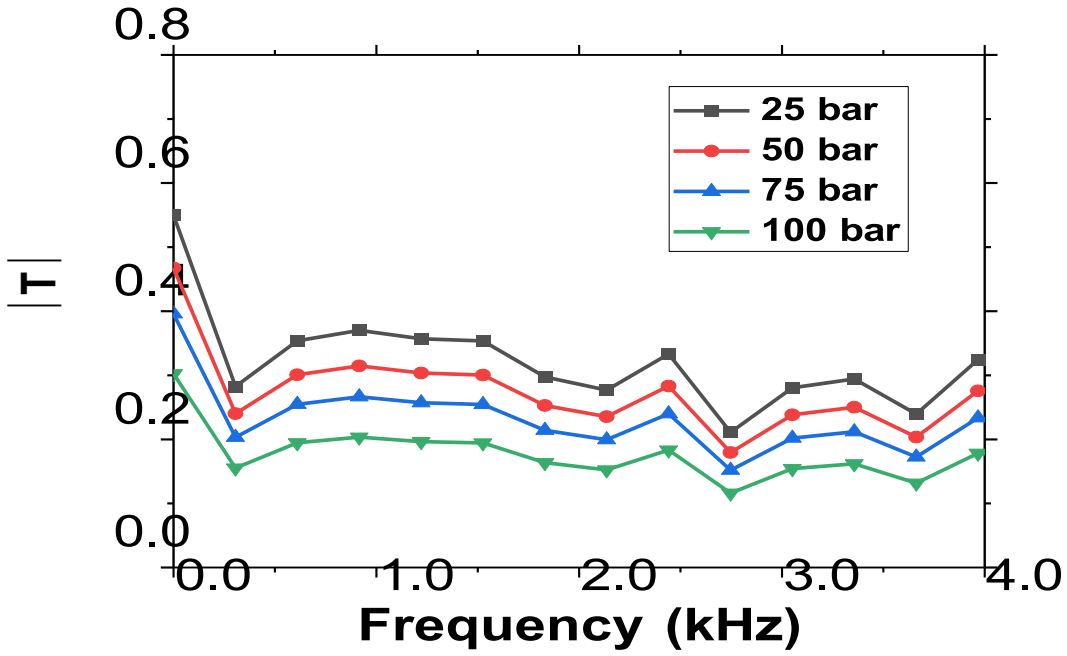


Figure 4.4: Effect of compaction pressure on the acoustic transmission coefficient of the CSL-WHA (samples M-2, M-6, M-10 and M-14).

4.7 Effect of compaction pressure on intrinsic acoustical properties

Figure 4.5 shows the variation of the microstructural non-acoustical parameters of the blocks as a function of the compression pressure and concentration of WHA.

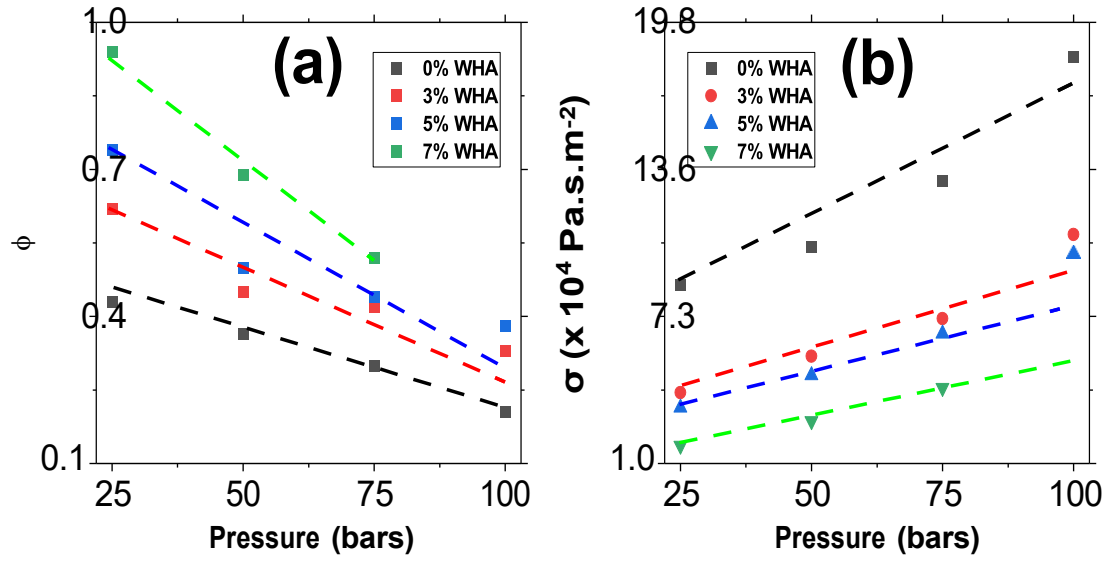


Figure 4.5: Plots of the intrinsic acoustical parameters: (a) porosity ϕ, and (b) airflow resistivity σ against compaction pressure.

While the porosity increased with increase in the concentration of WHA, it decreased with increase in the compaction pressure (Figure 4.5a). This can be attributed to the decrease in the volume of the voids with increase in the compaction pressure. Venkatarama (2012) also reported the decrease in the porosity of CSBs with increase in the compaction pressure. The airflow resistivity increased with increase in the compaction pressure (Figure 4.5b). This increase in air resistivity can be explained by the decrease in the porosity and decrease in the pore size as compaction pressure increases. The high frequency parameters (tortuosity, viscous characteristic lengths and thermal permeability) could not be obtained with enough precision for compaction pressures higher than 25 bars, because the data involved was not sensitive enough to reflect their variation in order to recover them correctly. The viscous characteristic length of the CSL-WHA blocks decreases with increase in compaction pressure. This is due to the fact that increasing the compaction pressure reduces the volume of voids, increases the contact surface between the grains and subsequently leads to a reduction in pore size thereby decreasing the Λ. This results in a poor signal to noise ratio for these high frequency parameters. They also require more data points.

CHAPTER FIVE
CONCLUSION AND RECOMMENDATION

5.1 Introduction

This chapter provides a comprehensive overview of the key findings derived from this study, delving into their implications and offering insightful recommendations for future research endeavors.

5.2 Conclusion

5.2.1 General Conclusion

The primary objective of this study centered on exploring the acoustical attributes of Compressed Soil Blocks (CSBs) with lime and Water Hyacinth Ash (WHA) binders. This encompassed a comprehensive investigation into material development, parameter assessment, the effects of varying binder concentrations, and the influence of compaction pressure. The study also delved into the feasibility of acoustical modeling for parameter retrieval, ultimately evaluating the potential of CSL-WHA blocks to meet specified acoustic requirements

A simple acoustic test-rig, composed of water pipes configured to form an extended long waveguide, was meticulously assembled at the Physics department laboratory in Maseno University. This test-rig played a crucial role in characterizing the acoustical parameters of CSL-WHA samples, with a focus on varying percentages of lime and WHA. The study, therefore, not only contributed to a deeper understanding of the acoustical characteristics of these samples but also showcased the practical implementation of a purpose-built test apparatus for comprehensive acoustic analysis within the university setting.

The study demonstrated that porosity serves as a crucial design parameter in optimizing the acoustical and structural performance of compressed soil blocks stabilized with lime and water hyacinth ash (CSL-WHA). Through detailed experimental characterization and inverse modeling, it was shown that porosity is significantly influenced by binder composition and compaction pressure. Although higher WHA content generally improves pore volume and connectivity,

beneficial for sound absorption, it tends to exceed the optimal porosity window of 0.26 to 0.35, thereby compromising material integrity. Notably, formulation M-14 (7% lime, 3% WHA at 100 bars) was found to strike a favorable balance, achieving porosity values within or near the target range similar to control formulations M-5 (10% lime, 0% WHA at 50 bars), M-9 (10% lime, 0% WHA at 75 bars) and M-13 (10% lime, 0% WHA at 100 bars).

These mixes also exhibited complementary acoustic parameters, including airflow resistivity, tortuosity ranging from 1.4 to 2.0, and viscous characteristic lengths around 11–17 μm, values that align with established benchmarks for efficient low-frequency damping. Collectively, the results confirm that moderate WHA incorporation (≤5%) paired with elevated compaction pressure (≥75 bar) offers a practical pathway for tailoring CSL-WHA blocks toward acoustical effectiveness without compromising mechanical resilience.

Ultimately, this research underscores the significance of binder–pressure synergy in developing sustainable materials that possess both structural utility and sound absorption capabilities. It provides a foundation for future exploration into eco-friendly construction technologies that address acoustic comfort and environmental performance.

5.2.2 Impact and Contribution of the Study

This research advances the field of sustainable construction by introducing compressed soil blocks stabilized with lime and water hyacinth ash (CSL-WHA) as viable acoustic and structural materials. The study establishes several novel insights and methodological innovations:

- **Parametric Control of Porosity**: The research demonstrates that porosity in CSL- WHA blocks can be precisely tuned using binder ratios and compaction pressure. This provides a strategic pathway for balancing structural resilience with acoustic performance, especially for values below 0.35, which ensures mechanical integrity.
- **Benchmarking Acoustic Parameters for Eco-Materials**: Through inverse modeling, the study introduces reference ranges for airflow resistivity, tortuosity, and viscous

characteristic length specific to WHA-lime systems. These benchmarks expand the characterization of bio-based building materials within acoustics research.

- **Methodological Innovation in Acoustic Identification**: The adoption of Julia-based inverse modeling for non-destructive characterization marks a shift towards computationally efficient and reproducible techniques. This methodological contribution strengthens the rigor of acoustic evaluation in sustainable materials research.
- **Valorization of Invasive Biomass**: Unlike prior studies centered on WHA's chemical role, this work pioneers its application in acoustic damping, highlighting its potential in low-frequency sound mitigation for partitioning systems in eco-buildings.
- **Design Mapping of Performance Trade-Offs**: The study introduces a trade-off matrix aligning acoustic efficiency with mechanical strength across formulation regimes, enabling tailored application in modular construction components such as façade inserts and partition walls.
- **Foundation for Localized Standardization:** By aligning retrieved acoustic properties with ISO 9053 and AFNOR NF S31-119, the research supports the establishment of region-specific standards for WHA-based construction materials in East Africa and other tropical regions.

5.3 Recommendations

5.3.1 Possible applications

Drawing on the study's optimized formulations, several potential applications emerge that align with structural performance, acoustic damping, and circular economy principles.

CSL-WHA blocks are suitable for use in internal partition walls in residential buildings, schools, and healthcare facilities where speech privacy, noise control, and thermal moderation are desired. Their capacity to absorb sound, especially in low-to-mid frequency ranges, makes them valuable in creating quieter, healthier indoor environments. Additionally, blocks with higher WHA content and increased tortuosity show promise in low-frequency acoustic absorber panels,

applicable in community halls, music rooms, or areas exposed to mechanical noise.

In external applications, façade systems constructed with lime-rich CSL-WHA blocks compacted at ≥100 bar provide structural resilience alongside passive thermal and sound regulation. These blocks are ideal for climate-sensitive and high-noise zones, particularly in low-rise housing and green-certified developments. Their mechanical integrity and acoustic permeability can be further leveraged in modular components.

Beyond functional design, the valorization of water hyacinth ash as a binder introduces a strong sustainability dimension. The use of WHA addresses aquatic biomass overgrowth while promoting green material development rooted in waste transformation and local resource utilization. Therefore, CSL-WHA blocks contribute meaningfully to affordable housing strategies, bioclimatic architecture, and eco-infrastructure programs, particularly in lake-region settlements and rural communities.

Generally, the study positions CSL-WHA blocks as multifunctional materials that bridge acoustics, sustainability, and structural performance, supporting global initiatives in circular construction, climate resilience, and inclusive building innovation.

5.3.2 Further Investigation

i. Comparative Analysis:

Conduct a detailed comparative analysis of the acoustical properties of CSL-WHA blocks against conventional construction materials (e.g., concrete, traditional earth blocks). Evaluate performance to identify strengths and areas for improvement.

ii. Environmental Impact Assessment:

Undertake a comprehensive environmental impact assessment comparing CSL-WHA blocks to conventional cement-based materials. Consider factors such as CO2 emissions, energy consumption, and overall sustainability.

iii. Long-term Durability Study:

Initiate a rigorous long-term durability study to observe the evolution of acoustical properties in

CSL-WHA blocks over time. Assess factors like weathering, wear and tear, and aging to ensure sustained and reliable performance.

iv. Soil Composition Correlation:

Address the existing gap by researching the correlation between soil composition, Atterberg limits, and expected acoustic characteristics. Develop design charts that provide guidance on the relationship between these factors, aiding in block production.

v. Optimization of Production Process:

Investigate methods to optimize the production process of CSL-WHA blocks. Focus on enhancing efficiency, reducing waste, and ensuring cost-effectiveness without compromising acoustical properties.

vi. Integration of Innovative Technologies:

Explore the integration of innovative technologies, such as additives or surface treatments, to enhance specific acoustical properties of CSL-WHA blocks. This exploration could lead to novel applications in specialized construction scenarios.

vii. Community Perception and Acceptance:

Gauge community perception and acceptance of CSL-WHA blocks through surveys or interviews. Assess factors including acoustical properties, affordability, and ease of use. Obtain valuable insights to inform real-world applications and enhance community adoption.

REFERENCES

Abana, E., Vega, W., Gacias, J., Rañon, P. J., Talattad, J. D., Orata, H., & Perez, J. (2021). Pulverized water hyacinth as an admixture for concrete. *International Journal of Integrated Engineering, 13*(4), 298–303. https://doi.org/10.30880/ijie.2021.13.04.028

Adam, E. A., & Jones, P. J. (1995). *Thermophysical properties of stabilised soil building blocks*. *Building and Environment*, 30(2), 245–253. https://doi.org/10.1016/0360-1323(94)00041-P

Adamczyk, A. (2015). Structural studies of aluminosilicate gels. *Materials Science-Poland, 33*(4), 732–741. https://doi.org/10.1515/msp-2015-0109

AFNOR. (1993). *Soils: Investigation and testing—Determination of Atterberg's limits—Liquid limit test using Casagrande apparatus—Plastic limit on rolled thread*. AFNOR.

Ahmed, S., Abdel, H., & Yasser, A. G. F. (2015). Impact of water hyacinth on properties of concrete made with various gravel to dolomite ratios. In *Proceedings of the Third International Conference on Advances in Civil, Structural and Mechanical Engineering (CSM 2015)*.

Akpokodje, E. G. (1985). The stabilization of some arid zone soils with cement and lime. *Quarterly Journal of Engineering Geology*, *18*(2), 173–180.

Alavez-Ramirez, R., Montes-Garcia, P., Martínez-Reyes, J., Altamirano-Juárez, D. C., & Gochi-Ponce, Y. (2012). The use of sugarcane bagasse ash and lime to improve the durability and mechanical properties of compacted soil blocks. *Construction and Building Materials*, *34*, 296–305.

Alireza, M., & Mohsen, N. (2020). A decision support tool for the cement industry to select energy efficiency measures. *Energy Strategy Reviews*, *28*, Article 100458. https://doi.org/10.1016/j.esr.2020.100458

Allard, J. F., & Atalla, N. (2009). *Propagation of sound in porous media: Modelling*

soundabsorbing materials. J. Wiley & Sons.

Allard, J. F., & Champoux, Y. (1992). New empirical equations for sound propagation in rigid frame fibrous materials. *Journal of the Acoustical Society of America, 91*(6), 3346–3353.

American Association of State Highway and Transportation Officials. (2012). *Classification of soils and soil-aggregate mixtures for highway construction purposes* (M145-91). American Association of State Highway and Transportation Officials.

American Society for Testing and Materials. (2000). *Standard practice for classification of soils for engineering purposes (Unified soil classification system)* (ASTM D2487-17). American Society for Testing and Materials.

American Society for Testing and Materials. (2007). *Standard test methods for particle-size analysis of soils* (ASTM D422-63). American Society for Testing and Materials.

American Society for Testing and Materials. (2010). *Standard test methods for liquid limit, plastic limit, and plasticity index of soils* (ASTM D4318-10e1). https://www.astm.org/standards/D4318.htm

American Society for Testing and Materials. (2020). *Standard test methods for physical testing of quicklime, hydrated lime, and limestone* (ASTM C110-20). American Society for Testing and Materials.

Aquaaid. (2021). *The role of calcium in the soil*. https://aquaaid.eu/wp-content/uploads/2021/04/Verdecal-G-2021.pdf

Arumala, J., & Gondal, T. (2007). Compressed earth building blocks for affordable housing. In *Proceedings of the Construction and Building Research Conference of the Royal Institution of Chartered Surveyors*.

Auriault, J.-L. (1991). Heterogeneous medium: Is an equivalent macroscopic description possible?*International Journal of Engineering Science*, *29*(7), 785–795.

Baciocchi, R. (2017). Carbonation of industrial residues for CCUS: Fundamentals, energy requirements, and scale-up opportunities. In *CO_2 Summit III: Pathways to carbon*

capture,utilization, and storagedeployment (ECI Symposium Series). https://dc.engconfintl.org/co2_summit3/15

Bassett, J., Denney, R. C., Jeffrey, G. H., & Mendham, J. (1986). *Vogel's textbook of quantitative chemical analysis*. Longman Group.

Bell, F. G. (1993). *Engineering treatment of soil: Soil stabilization*. E and FN Spon

Bell, F. G. (1996). Lime stabilization of clay minerals and soils. *Engineering Geology*, *42*(4), 223–237.

Ben Mansour, M., Ogam, E., Fellah, Z. E. A., Amel, S. C., Ahmed, J., & Ben Jabrallah, S. (2016). Characterization of compressed earth blocks using low frequency guided acoustic waves. *The Journal of the Acoustical Society of America*, *139*, 2551.

Ben Mansour, M., Ogam, E., Jelidi, A., Cherif, A. S., & Ben Jabrallah, S. (2017). *Influence of compaction pressure on the mechanical and acoustic properties of compacted earth blocks: An inverse multi-parameter acoustic problem*. *Applied Acoustics*, 125, 128–135. https://doi.org/10.1016/j.apacoust.2017.04.017

Beranek, L. L. (1942). Acoustic impedance of porous materials. *Journal of the Acoustical Society of America*, *13*(3), 248–260.

Bezanson, J., Karpinski, S., Shah, V. B., Edelman, A. (2012). Julia: A fast dynamic language for technical computing. https://doi.org/10.48550/arXiv.1209.5145

Bhatia, S., & Perlmutter, D. D. (1983). Effect of the product layer on the kinetics of the CO_2-lime reaction. *AIChE Journal*, *29*(1), 79–86. https://doi.org/10.1002/aic.690290111

Binici, H., Akogan, O., & Shah, T. (2005). Investigation of fiber reinforced mud brick as a building material. *Construction and Building Materials*, *19*(4), 313–318.

Binici, H., Aksogan, O., Bakbak, D., Kaplan, H., & Isik, B. (2009). Sound insulation of fibre reinforced mud brick walls. *Construction and Building Materials, 23*(2), 1035–1041. https://doi.org/10.1016/j.conbuildmat.2008.05

Biot, M. A. (1956). The theory of propagation of elastic waves in fluid-saturated porous solid. I. Low frequency range. *Journal of the Acoustical Society of America*, *28*(2), 168–178.

Biot, M. A. (1956). The theory of propagation of elastic waves in fluid-saturated porous solid. II. Higher frequency range. *Journal of the Acoustical Society of America*, *28*(2), 179–191.

Biot, M. A. (1962). Mechanics of deformation and acoustic propagation in porous media. *Journal of Applied Physics*, *33*(5), 1482–1498.

Bogas, J. A., Silva, M., & Gomes, M. D. G. (2018). Unstabilized and stabilized compressed earth blocks with partial incorporation of recycled aggregates. *International Journal of Architectural Heritage*, *12*(3), 1–16.

Bolton, J. S., & Hong, K. (2009). Inverse characterization of poro-elastic materials based on acoustical input data. *Publications of the Ray W. Herrick Laboratories*. Paper 30. http://docs.lib.purdue.edu/herrick/30

Brown, N., Melon, M., Montembault, V., Castagnède, B., Lauriks, W., & Leclaire, P. (1996). *Evaluation of the viscous characteristic length of air-saturated porous materials from the ultrasonic dispersion curve*. Comptes Rendus de l'Académie des Sciences – Series Iib: Mechanics. Retrieved from HAL archive

Bureau of Indian Standards. (1967). *IS:1727: Methods of test for pozzolanic materials*. Bureau of Indian Standards.

Bureau of Indian Standards. (1969). *IS:1350 (Part III)-1969: Methods for test of coal and coke – Determination of sulphur*. Bureau of Indian Standards.

Bureau of Indian Standards. (1969). *IS:1350 (Part III)-1969: Methods for test of coal and coke - Determination of sulphur*. Bureau of Indian Standards.

Bureau of Indian Standards. (1995). *IS:4031 (Part 4): Methods of physical tests for hydraulic cement - Determination of consistency of standard cement paste*. Bureau of Indian Standards.

Bureau of Indian Standards. (2013). *IS:8112: Ordinary Portland cement, 43 grade – Specification*. Bureau of Indian Standards.

Campo, F. P., Tua, C., Biganzoli, L., Pantini, S., & Grosso, M. (2021). Natural and enhanced carbonation of lime in its different applications: A review. *Environmental Technology Reviews, 10*(1), 224–237. https://doi.org/10.1080/21622515.2021.1982023

Champoux, Y., & Allard, J.-F. (1991). Dynamic tortuosity and bulk modulus in air-saturated porous media. *Journal of Applied Physics, 70*(4), 1975–1979.

Champoux, Y., & Stinson, M. R. (1992). On acoustical models for sound propagation in rigid frame porous materials and the influence of shape factors. *Journal of the Acoustical Society of America, 92*(2), 1120–1131.

Champoux, Y., Stinson, M. R., & Daigle, G. A. (1991). Air-based system for the measurement of porosity. *Journal of the Acoustical Society of America*, *89*(2), 910–916.

Cizer, Ö., Rodriguez-Navarro, C., Ruiz-Agudo, E., Elsen, J., van Gemert, D., & van Balen, K. (2012). Phase and morphology evolution of calcium carbonate precipitated by carbonation of hydrated lime. *Journal of Materials Science*, *47*(17), 6151–6165. https://doi.org/10.1007/s10853-012-6535-7

Danso, H. (2018). *Suitability of soil for earth construction as a building material*. Crimson Publishers.

Das, N., & Singh, S. (2016). Evaluation of water hyacinth stem ash as pozzolanic material for use in blended cement. *Journal of Civil Engineering, Science and Technology, 7*(1), 1–8. https://doi.org/10.33736/jcest.150.2016

Despotou, E., Shtiza, A., Schlegel, T., & Verhelst, F. (2016). Literature study on the rate and mechanism of carbonation of lime in mortars. *Mauerwerk*, *20*, 124–137.https://doi.org/10.1002/dama.201500674 earthtek/

European Lime Association. (2019). *A competitive and efficient lime industry*. https://www.eula.eu

Fackler, C. J. (2014). *Bayesian model selection for analysis and design of multilayer sound*

absorbers (Doctoral dissertation, Rensselaer Polytechnic Institute). ProQuest Dissertations & Theses Global.

Fellah, M., Fellah, Z. E. A., Mitri, F. G., Ogam, E., & Depollier, C. (2013). Transient ultrasound propagation in porous media using Biot theory and fractional calculus: Application to human cancellous bone. *Journal of the Acoustical Society of America*, *133*(3), 1867–1881.

Fellah, Z. E. A., & Depollier, C. (2000). Transient acoustic wave propagation in rigid porous media: A time-domain approach. *Journal of the Acoustical Society of America*, *107*(1), 683–688.

Geiman, C. M. (2005). *Stabilization of soft clay subgrades in Virginia: Phase I laboratory study* (Master's thesis, Virginia Polytechnic Institute and State University). ProQuest Dissertations & Theses Global.

Gle, G., Gourdon, E., & Arnaud, L. (2011). *Acoustical properties of materials made of vegetable particles with several scales of porosity*. Construction and Building Materials, 25(4), 1712-1718. https://doi.org/10.1016/j.apacoust.2010.11.003

Goel, G., & Kalamdhad, A. S. (2018). A practical proposal for 65tilization of water hyacinth: Recycling in fired bricks. *Journal of Cleaner Production, 190*, 261–271. https://doi.org/10.1016/j.jclepro.2018.04.179

Groby, J.-P., Ogam, E., De Ryck, L., Sebaa, N., & Lauriks, W. (2010). Analytical method for the ultrasonic characterization of homogeneous rigid porous materials from transmitted and reflected coefficients. *Journal of the Acoustical Society of America*, *127*(2), 764–772.

Guettala, A., Houari, H., Mezghiche, B., & Chebili, R. (2002). Durability of lime stabilized earth blocks. *Courrier du Savoir*, *2*(1), 61–66.

Holzer, L., Neumann, M., & Gasser, P. (2023). *Tortuosity–Porosity Relationships: Review of Empirical Data from Literature*. In Springer Series in Materials Science. Springer. https://doi.org/10.1007/978-3-031-27485-9_3

Horoshenkov, K. V. (2017). A review of acoustical methods for porous material characterization. *International Journal of Acoustics and Vibration*, *22*(1), 92–103.

International Organization for Standardization. (1991). *ISO 9053:2001 Acoustics—Materials for acoustical applications—Determination of airflow resistance*. Geneva, Switzerland: ISO

International Organization for Standardization. (2002). *ISO 4590: Rigid cellular plastics – Determination of the volume percentage of open cells and of closed cells*. International Organization for Standardization.

Ipinge, I. L. (2012). *Durability of compressed stabilized earth blocks* (Master's thesis, University of the Witwatersrand). Johannesburg.

Jaouen, L. (2016). *The acoustic characterization of porous media and its standards*. François-Xavier Becot, Fabien Chevillotte, & Matelys.

Johnson, D. L., Koplik, J., & Dashen, R. (1987). Theory of dynamic permeability and tortuosity in fluid-saturated porous media. *Journal of Fluid Mechanics*, *176*, 379–402.

Kamal, M. A. (2023). Analyzing the potential of compressed earth blocks as a feasible and sustainable building material. *Architecture Engineering and Science*, *4*(2), Article 1183.

Kinuthia, J. M., Wild, S., & Jones, G. I. (1999). Effects of monovalent and divalent metal sulphates on consistency and compaction of lime-stabilized kaolinite. *Applied Clay Science*, *14*(1-3), 27–45.

Lafarge, D. (1993). *Sound propagation in porous materials having a rigid frame saturated by gas* (Doctoral dissertation, Université du Maine). ProQuest Dissertations & Theses Global.

Lafarge, D. (1993). *Sound propagation in porous materials having a rigid frame saturated by gas* (Unpublished doctoral dissertation). Université du Maine, Le Mans.

Lafarge, D. (1993). *Sound propagation in porous materials having a rigid frame saturated by gas* (Ph.D. thesis). Université du Maine, Le Mans, France.

Lafarge, D., Lemarinier, P., Allard, J. F., & Tarnow, V. (1997). Dynamic compressibility of air in porous structures at audible frequencies. *Journal of the Acoustical Society of America,*

102(4), 1995–2006. https://doi.org/10.1121/1.419690

Lai, Q. T., Habte, L., Thriveni, T., Seongho, L., & Ahn, J. W. (2021). COVID-19 impacts on climate change: Sustainable technologies for carbon capture, storage, and utilization (CCUS). In *Minerals, metals and materials series* (pp. 23–28). https://doi.org/10.1007/978-3-030-65257-9_3

Langaroudi, M. A. M., & Mohammadi, Y. (2018). Effect of nano-clay on workability, mechanical, and durability properties of self-consolidating concrete containing mineral admixtures. *Construction and Building Materials*, *191*, 619–634. https://doi.org/10.1016/j.conbuildmat.2018.10.044

Lefeuve-Mesgouez, G., Mesgouez, A., Ogam, E., Scotti, T., & Wirgin, A. (2013). Retrieval of the physical properties of an anelastic solid half space from seismic data. *Journal of Applied Geophysics, 88*, 70–82. https://doi.org/10.1016/j.jappgeo.2012.09.010

Lindh, P., & Lemenkova, P. (2023). Geotechnical properties of soil stabilized with blended binders for sustainable road base applications. *Construction Materials*, *3*(1), 110–126. https://doi.org/10.3390/constrmater3010008

Lindh, P., & Lemenkova, P. (2023). Laboratory experiments on soil stabilization to enhance strength parameters for road pavement. *Transport and Telecommunication, 24*(1), 73–82. Transport and Telecommunication Institute.

Ma, M. J., Xi, F. M., Ling, J. H., Wang, J. Y., & Quan, S. M. (2019). Research progress on mineral carbonation of carbon dioxide. *Chinese Journal of Ecology*, *38*, 3854–3863.

Malhotra, P. (2023). Atomic absorption spectroscopy. In *Analytical chemistry*. Springer. https://doi.org/10.1007/978-3-031-26757-4_6

Malhotra, V. M. (2004). Role of supplementary cementing materials and superplasticizers in reducing greenhouse gas emissions. In *Proceedings of the ICFRC International Conference on Fiber Composites, High-Performance Concrete, and Smart Materials* (pp. 489–499).

Chennai, India.

Malkanthi, S. N., Balthazaar, N., & Perera, A. A. D. A. J. (2019). Lime stabilization for compressed stabilized earth blocks with reduced clay and silt. *Case Studies in Construction Materials*, *12*, Article e00326. https://doi.org/10.1016/j.cscm.2019.e00326

Mallela, J., Von Quintus, P. H., Smith, K. L., & E. Consultants. (2004). *Consideration of lime stabilized layers in mechanistic-empirical pavement design*. The National Lime Association.

Matti, N., Jean-Philippe, G., Aroune, D., Olivier, D., Timo, L., & Tomi, H. (2016). Inverse acoustic characterization of rigid frame porous materials from impedance tube measurements. In *Sound intensity and inverse methods in acoustics: Paper ICA2016-533*.

Meso, C., Fellah, Z. E. A., Diallo, E. H. A., Ogam, E., & Valentin, M. (2025). *Determination of viscous and thermal characteristic lengths in rigid porous materials via ultrasonic and Brewster angle measurements*. *Journal of the Acoustical Society of America*, *157*(6), 4546–4558. https://doi.org/10.1121/10.0036922

Mishra, S., & Saddiqui, N. A. (2014). A review on environmental and health impacts of cement manufacturing emissions. *International Journal of Geology, Agriculture and Environmental Sciences*, *1*(1), 26–31.

Mo, L., & Panesar, D. K. (2012). Effects of accelerated carbonation on the microstructure of Portland cement paste containing reactive MgO. *Cement and Concrete Research*, *42*, 769–777.

Mohankumar, S. R., & Rakaraddy, P. G. (2018). Influence of magnesium chloride on plasticity characteristics of black cotton soil. *International Research Journal of Engineering and Technology (IRJET)*, *5*(6). https://www.irjet.net/archives/V5/i6/IRJET-V5I6368.pdf

Murugesh, V., & Balasundaram, N. (2017). Experimental investigation on water hyacinth ash as a partial replacement of cement in concrete. *International Journal of Civil Engineering*

and Technology (IJCIET), *8*(9), 1013–1018.

Mustapha, S., Mohamed, F., Zine El Abiddine, F., Ogam, E., & Claude, D. (2013). Acoustic characterization of porous materials with a rigid structure in the low frequency regime. In *Proceedings of the Fifth Biot Conference on Poromechanics* (pp. 193–199). Vienne, Austria.

Nagaraj, H. B., Rajesh, A., & Sravan, M. V. (2016). Influence of soil gradation, proportion and combination of admixtures on the properties and durability of CSEBs. *Construction and Building Materials, 110*, 135–144. https://doi.org/10.1016/j.conbuildmat.2016.02.023

Nagaraj, H. B., Sravan, M. V., Arun, T. G., & Jagadish, K. S. (2014). Role of lime with cement in long-term strength of compressed stabilized earth blocks. *International Journal of Sustainable Built Environment*, *3*(1), 54–61.

Nagaraj, H. B., Sravan, M. V., Arun, T. G., & Jagadish, K. S. (2014). Role of lime with cement in long-term strength of compressed stabilized earth blocks. *International Journal of Sustainable Built Environment, 3*(1), 54–61. https://doi.org/10.1016/j.ijsbe.2014.03.001

NASA. (2020). *The causes of climate change*. Retrieved from https://climate.nasa.gov/causes/

Nimmo, J. R. (2004). *Porosity and pore size distribution*. In Hillel, D. (Ed.), *Encyclopedia of Soils in the Environment* (Vol. 3, pp. 295–303). Elsevier. https://wwwrcamnl.wr.usgs.gov/uzf/abs_pubs/papers/nimmo.04.encyc.por.ese.pdf

Nshimiyimana, P., Bui, Q. B., & Chanut, M. A. (2023). *Optimisation of Compressed Earth Blocks (CEBs) Using Natural Origin Materials: A Systematic Literature Review*. University of Liège.

Ocola, L., & Huaco, P. (2005). Seismic response of adobe buildings in Peruvian territory: 1974 –2001 earthquakes. In *Proceedings of SismoAdobe2005* [CD-ROM]. Lima, Peru.

Ocola, L., & Huaco, P. (2005). Seismic response of adobe buildings in Peruvian territory: 1974–2001 earthquakes. In *Proceedings of the SismoAdobe 2005* [CD-ROM]. Lima.

Ogam, E., Fellah, Z. E. A., Ogam, G., Ongwen, N. O., & Oduor, A. O. (2021). Investigation of long acoustic waveguides for the very low frequency characterization of monolayer and stratified air-saturated poroelastic materials. *Applied Acoustics, 182*, 108200. https://doi.org/10.1016/j.apacoust.2021.108200

Okwadha, G. D. O., & Makomele, D. M. (2018). Evaluation of water hyacinth extract as an admixture in concrete production. *Journal of Building Engineering, 16*, 129–133. https://doi.org/10.1016/j.jobe.2018.01.002

Onchiri, R., Kiprotich, J., Sabuni, B., & Claude, B. (2014). Use of sugarcane bagasse ash as a partial replacement for cement in stabilization of self-interlocking earth blocks. *International Journal of Civil Engineering and Technology (IJCIET)*, *5*(10), 124–130.

Ongwen, N. O., & Alruqi, A. B. (2023). Acoustics of compressed earth blocks bound using sugarcane bagasse ash and water hyacinth ash. *Applied Sciences, 13*(14), 8223. https://doi.org/10.3390/app13148223

Pan, S. Y., Chang, E. E., & Chiang, P.-C. (2012). CO_2 capture by accelerated carbonation of alkaline wastes: A review on its principles and applications. *Aerosol and Air Quality Research*, *12*, 770–791.

Pan, S. Y., Chen, Y. H., Fan, L. S., Kim, H., Gao, X., Ling, T. C., Chiang, P. C., Pei, S. L., & Gu, G. (2020). CO_2 mineralization and utilization by alkaline solid wastes for potential carbon reduction. *Nature Sustainability, 3*(6), 399-405. https://doi.org/10.1038/s41893-020-0486-9

Panesar, D. K., & Mo, L. (2013). Properties of binary and ternary reactive MgO mortar blends subjected to CO_2. *Cement and Concrete Composites, 38*, 40-49.

Panneton, R., & Olny, X. (2006). Acoustical determination of the parameters governing viscous dissipation in porous media. *Journal of the Acoustical Society of America, 119*(4), 2027-2040.

Philip, S., & Rakendu, R. (2020). Thermal insulation materials based on water hyacinth for application in sustainable buildings. *Materials Today: Proceedings*. https://doi.org/10.1016/j.matpr.2020.06.219

Piattoni, Q., Quagliarini, E., & Lenci, S. (2011). Experimental analysis and modelling of the mechanical behaviour of earthen bricks. *Construction and Building Materials, 25*(4), 2067–2075. https://doi.org/10.1016/j.conbuildmat.2010.11.039

Powell, D. (2021). Benefits of compressed earth blocks. *Green BuildingCanada*. https://greenbuildingcanada.ca/2012/benefits-compressed-earth-blocks-dan-powell-

Pride, S. R., Moran, F. D., & Gangi, A. F. (1993). Drag forces of porous-medium acoustics.*Physical Review B, 47*(7), 4964-4978. https://doi.org/10.1103/PhysRevB.47.4964

Raheem, A., Bello, O., & Makinde, O. (2010). A comparative study of cement and lime stabilized lateritic interlocking blocks. *The Pacific Journal of Science and Technology, 11*, 27–34.

Renforth, P. (2019). The negative emission potential of alkaline materials. *Nature Communications, 10*, Article 1401. https://doi.org/10.1038/s41467-019-09475-5

Roychand, R., Li, J., De Silva, S., Saberian, M., Law, D., & Pramanik, B. K. (2021). Development of zero cement composite for the protection of concrete sewage pipes from corrosion and fatbergs. *Resources, Conservation and Recycling, 164*, 105166. https://doi.org/10.1016/j.resconrec.2020.105166

Samari, M., Ridha, F., Manovic, V., Macchi, A., & Anthony, E. J. (2020). Direct capture of carbon dioxide from air via lime-based sorbents. *Mitigation and Adaptation Strategies for Global Change, 25*(1), 25–41. https://doi.org/10.1007/s11027-019-9845-0

Sebaa, N., Zine El Abiddine, E. A., Fellah, M., Lauriks, W., & Depollier, C. (2005). Measuring flow resistivity of porous material via acoustic reflected waves. *Journal of Applied Physics, 98*, 1–10. https://doi.org/10.1063/1.2099510

Sherwood, P. (1993). *Soil stabilization with cement and lime: State of the art review*. Transport

Research Laboratory. HMSO.

Shyam, K. S., & Murugesh, V. (2017). Experimental study on strength of water hyacinth as partial replacement of cement in concrete. *International Journal for Research in Applied Sciences and Engineering Technology, 5*(10).

Snæbjörnsdóttir, S., Sigfússon, B., Marieni, C., Goldberg, D., Gislason, S. R., & Oelkers, E. H. (2020). Carbon dioxide storage through mineral carbonation. *Nature Reviews Earth & Environment, 1*(2), 90–102. https://doi.org/10.1038/s43017-019-0011-8

Sri Lanka Standards Institution. (2009). *Sri Lanka standard specification for compressed stabilized earth blocks: Part 1* (SLS 1382).

Terrei, R. L., Epps, J. A., Barenberg, E. J., Mitchell, J. K., & Thompson, M. R. (1979). *Soil stabilization in pavement structures: A user manual* (FHWA Research Report No. FHWA-IP-80-2). Federal Highway Administration.

Terrei, R., Epps, J., Barenberg, E., Mitchell, J., & Thompson, M. (1984). *Soil stabilization in pavement structures: A user's manual (Vol. 2, Moisture design considerations)*. Federal Highway Administration.

U.S.Geological Survey. (2018). *Cement statistics and information*. https://www.usgs.gov/minerals/pubs/commodity/cement/mcs-2016-cemen.pdf

Venkatarama, R. V. B. (2012). *Stabilized soil blocks for structural masonry construction*. Woodhead Publishing Limited.

Visser, D. (2024). *Atomic Absorption Spectroscopy: Principles and Applications*. Technology Networks. https://www.technologynetworks.com/analysis/articles/atomic-absorption-spectroscopy-principles-and-applications-356829

Williams, C., Goodhew, S., Griffiths, R., & Watson, L. (2010). The feasibility of earth block masonry for building sustainable walling in the United Kingdom. *Journal of Building Appraisal, 6*(2), 99–108. https://doi.org/10.1057/jba.2010.15

Zielinski, T. D. (2015). Normalized inverse characterization of sound absorbing rigid porous

media. *Journal of the Acoustical Society of America, 137*(6), 3232–3243. https://doi.org/10.1121/1.4914861

Zine El Abiddine, F., Fellah, M., Sebaa, N., Lauriks, W., & Depollier, C. (2006). Measuring flow resistivity of porous materials at low frequencies via acoustic transmitted waves. *Journal of the Acoustical Society of America, 119*(4), 1926–1928. https://doi.org/10.1121/1.2179749

APPENDICES

JULIA SCRIPTS USED FOR COMPUTATION

APPENDIX I: A SCRIPT TO COMPUTE TRANSMISSION COEFFICIENT FROM THE DATA

```
using DelimitedFiles,XLSX ENV["GKS_ENCODING"] = "utf-8"
using Plots;
np = pyimport("numpy")
function coeffTrans( fr,por, resist, lambd,rapp, alphinf, k00p,d) #d = 0.2e-1;
#fr=range(0,step=10,stop=1000); w = (2*pi.*fr);
yy = 1.401;
Pr = .713;
P0 = 101325.;
rho0 = 1.297;
c0 = 344;
Kf0 = yy*P0; visc0 = 0.178e-4;
lambdp = rapp*lambd;
k00 = visc0/resist;
Gw2 = sqrt.(1 .+(4.0*im)*k00p^2*rho0.*w*Pr/(visc0*por^2*lambdp^2)); bet = yy .-(yy-1)./(1 .-
im*visc0*por.*Gw2./(w*rho0*k00*Pr));
Kf = Kf0./bet;
Gw1 = sqrt.(1 .+(4.0*im)*alphinf.^2*k00^2*rho0.*w/(visc0*por^2*lambd^2)); alphtort =
(alphinf.*(1 .-im*visc0*por.*Gw1./(w*alphinf*rho0*k00)));
k0 = w./c0;

rho2 = (rho0.*alphtort); c11 = (sqrt.(Kf./rho2)); k2 = w./c11;
z0 = rho0*c0; z2 = rho2.*c11; Z = z2./z0;
return (2*por*Z.*exp.(im*k0*d)./((2)*por.*Z.*cos.(k2*d) .+im*(por^2 .+Z.^2).*sin.(k2*d)));
end
function main()

#Initialization of porous parameters por0 = 0.60; resist0 = 2*1.2e4; lambd0=4.5e-06;  alphinf0 =
1.01;
k00p0 =6.0e-1;          rapp0=3.0;#lambdp/lambda
```

```
d=2.0e-2; # thickness

#Read experimental data TC from the file generated by the other program global xf
=XLSX.openxlsx("S1_trcoeff.xlsx",enable_cache=false) #freq=range(0,step=10,stop=3500);
fre=np.array(xf[1]["A2:A20"]);#an array of frequencies where to compute
AmpExp=np.array(xf[1]["B2:B20"]);
fr=1:50:3500;

coeftr=coeffTrans(fr,por0,resist0, lambd0, rapp0,alphinf0, k00p0,d) ampl=abs.(coeftr);
PtcExp=plot(fre,AmpExp,ylims=(0,1),xlabel="Frequency
(Hz)",ylabel=("|T|"),legend=:topright,line=(:red, 0.5, 6, :scatter),marker =
(:star8),lw=0.02,grid=false, label
=("Experiment"),xtickfontsize=16,ytickfontsize=16,xguidefontsize=16,yguidefontsize=16,fra
mestyle=:box )
global ptc=plot!(fr,ampl,ylims=(0,1),xlabel="Frequency
(Hz)",ylabel=("|T|"),legend=:topright,line=(:blue, 0.5, 6, :dash),marker = ([:hex
:d]),lw=0.02,grid=false, label

=("Model"),xtickfontsize=16,ytickfontsize=16,xguidefontsize=16,yguidefontsize=16,framest
yle=:box ,xlims=(0,3500))
end main ()
```

APPENDIX II: SCRIPT TO COMPUTE COHERENCE OF THE SIGNAL

```
ENV["GKS_ENCODING"]="utf-8"
using LaTeXStrings using DelimitedFiles using CSV,XLSX using Plots
using DataFrames using PyCall
np = pyimport("numpy") #
#Signal processing #Pkg.add("DSP")
#Pkg.add("FFTW") using DSP
using FFTW #
# ----------
  ----------

df = CSV.read("M1 I.csv",DataFrame,header=1:3); n1=390000;n2=800000;
t1=df[n1:n2,1]*1e-3;#range time in milliseconds

w_out=df[n1:n2,2]*1e-3;

df = CSV.read("M1 T.csv",DataFrame,header=1:3); w_sample=df[n1:n2,2]*1e-3;
#  ----------
#  ----------
Ls=length(t1); L=nextpow(2,Ls/2); t=np.array(t1); sig1=np.array(w_out);
sig2=np.array(w_sample); #sig1w=sig1[:].*hanning(Ls) #sig2w=sig2[:].*hanning(Ls)
f_sig1=fft(sig1); f_sig2=fft(sig2);
fs=1/(t[2]-t[1])
p1=plot(t,sig1 ,xlabel="Time (s)",ylabel="Amplitude (Arb. units)",label="Without Sample",lw
= 3,xtickfontsize=12,ytickfontsize=12);
#plot!(dtheo1[:,1],300 .+ 8*dtheo1[:,2],label="Without",lw = 4,linestyle = :dot);
p2=plot!(t1, sig2,label="With Sample",ylims=(-80e-3,80e-3),lw = 4,linestyle =
:dashdot,line=(:red, 0.5, 6, :solid));

#Signal processing #xdft1 = f_sig1; #M=floor(Int,N/2) xdft1= f_sig1[1:Ls];
psdx1=1/(2*pi*Ls)*abs.(xdft1).^2; psdx1[2:end-1]=2*psdx1[2:end-1]; xdft2= f_sig2[1:Ls];
psdx2=1/(2*pi*Ls)*abs.(xdft2).^2; psdx2[2:end-1]=2*psdx2[2:end-1];
#fr=fftfreq(length(x.Column1),fs); fr=fs*range(0,step=1,stop=L)/L; #p=plot(p1,p2)
savefig(p2, "test.png")
```

```
pf1=plot(fr[1:L],psdx1[1:L]/L,xlims=(1,7000),xlabel="Frequency (Hz)",ylabel=("Power
spectral density"),legend=:topright,line=(:red, 0.5, 6, :solid),lw=0.02,grid=false, label
=("Without
Sample"),xtickfontsize=16,ytickfontsize=16,xguidefontsize=16,yguidefontsize=16,framestyle
=:box);

pf2=plot!(fr[1:L],psdx2[1:L]/L,xlims=(1,7000),xlabel="Frequency (Hz)",ylabel=("Power
spectral density"),legend=:topright,line=(:green, 0.5, 6, :solid),lw=0.02,grid=false, label

=("WithSample"),xtickfontsize=16,ytickfontsize=16,xguidefontsize=16,yguidefontsize=16,fr
amestyle=:box);
#p_pow=plot(pf1,pf2)

#Calculating the transmission coefficient Sxx=f_sig1.*conj(f_sig1)/Ls^2;#Two-Sided  auto
Power Spectrum Sxy=f_sig1.*conj(f_sig2)/Ls^2;#Two-Sided cross Power Spectrum
Syy=f_sig2.*conj(f_sig2)/Ls^2;#Two-Sided cross Power Spectrum Ltc=500;#length
transmission coefficient
frfin=fr[1:Ltc]; Trcoef=Sxy[1:Ltc]./Sxx[1:Ltc]; Trcoeff=abs.(Trcoef);
#  ------------------------

#Calculating the wave velocity in the block #
Trcoeff_ang=unwrap(angle.(Trcoef)); deltT=Trcoeff_ang./(2*pi*frfin) Lb=2e-2;# thickness of
the block C0=340;#wave velocity in air phaseVel=Lb*C0./(Lb .- C0*deltT)

ptrc_vel=plot(frfin,phaseVel,xlims=(0,5000),ylims=(-300,1150);xlabel="Frequency
(Hz)",ylabel=("Phase Velocity (m/s)"),label=("S2"), line=(:red, 0.5, 6,
:solid),lw=0.02,grid=false,
xtickfontsize=16,ytickfontsize=16,xguidefontsize=16,yguidefontsize=16,framestyle=:box )
Trco=plot(frfin,Trcoeff,xlims=(0,5000),ylims=(0,1),xlabel="Frequency
(Hz)",ylabel=("|T|"),label=("S1"), line=(:red, 0.5, 6, :solid),lw=0.02,grid=false,
xtickfontsize=16,ytickfontsize=16,xguidefontsize=16,yguidefontsize=16,framestyle=:box )
s1=vec(sig1);

#spec_config = MTSpectrogramConfig{Float64}(length(s1), 256, 128; fs=fs); #mt_spec3 =
```

```
mt_spectrogram( s1, spec_config)
n=div(Ls, 2); nfft=nextfastfft(n); noverlap=div(n, 128);
pw1=welch_pgram(s1, n, noverlap; onesided=eltype(s1)<:Real, nfft, fs=fs) Y1 =
periodogram(s1; fs=fs,nfft=4*Ls) #plot(pw1.freq[:],abs.(pw1.power),xlims=(0,3000))
pw1=welch_pgram(s1, n, noverlap; onesided=eltype(s1)<:Real, nfft, fs=fs)
plot(pw1.freq[:],abs.(pw1.power),xlims=(0,3000))
ppw1=plot!(Y1.freq, (Y1.power),xlims=(0,3e3)) #Y2 = periodogram(vec(sig2); fs=fs)
s2=vec(sig2);Y2 = periodogram(s2; fs=fs,nfft=4*Ls);

#plot!(Y2.freq, DSP.pow2db.(Y2.power),xlims=(0,5e3))
pw2=welch_pgram(s2, n, noverlap; onesided=eltype(s1)<:Real, nfft, fs=fs)
plot(pw2.freq[:],abs.(pw2.power),xlims=(0,3000),line=(:red, 0.5, 6,

:solid),lw=0.02,grid=false,
xtickfontsize=16,ytickfontsize=16,xguidefontsize=16,yguidefontsize=16,framestyle=:box)
ppw2=plot!(Y2.freq, (Y2.power),xlims=(0,5e3),line=(:blue, 0.5, 6, :solid)) #dt, tbp, kspec, nf, p
= 1.0/fs, 3.5, 5, L/2, .90
two_signal1 = Matrix{Float64}(undef, 2, Ls) two_signal2 = Matrix{Float64}(undef, 2, Ls)
two_signal1[1, :] = s1;
two_signal1[2, :] = s2; nw = 1;
ntapers = 2 * nw - 1; window1=hamming(1024)
#mc=mt_coherence(two_signal; demean=true, fs=fs, freq_range = (0, 5000));
mt_config=MTConfig{Float64}(Ls; fs=fs,
nfft = nextpow(2, Ls), window = nothing, nw,
ntapers,
taper_weights = fill(1/ntapers, ntapers), onesided=eltype(s1)<:Real,  #onesided= false,
fft_flags = FFTW.MEASURE)

config = MTCrossSpectraConfig(2, mt_config; demean=true,freq_range=(0,5000))
mc=mt_cross_power_spectra(two_signal1, config);
two_signal2[1, :] = s1; two_signal2[2, :] = s1;
mc_prop=mt_cross_power_spectra(two_signal2,config);

amp=abs.(mc.power[1,2,:]./abs.(mc_prop.power[1,1,:])); # transmission coefficient
```

```
plot(mc_prop.freq[:],amp,ylims=(0,0.35),xlims=(0,3000),line=(:blue, 0.5,
6),lw=0.02,label=("MultiTaper crosspower spec"))
TrCoeff2=plot!(frfin,Trcoeff,xlims=(0,5000),ylims=(0,1),xlabel="Frequency
(Hz)",ylabel=("|T|"),label=("S2"), line=(:red, 0.5, 6, :solid),lw=0.02,grid=false,
xtickfontsize=16,ytickfontsize=16,xguidefontsize=16,yguidefontsize=16,framestyle=:box
)#nw=8;ntapers=2*nw;mt_pgram(s2; onesided=eltype(s2)<:Real, nfft=Ls, fs=fs2, nw=8,
ntapers=ceil(2nw), window=dpss(length(s2), nw, ntapers))# calculate coherency
#compute the coherence

config = MTCoherenceConfig{eltype(two_signal1)}(size(two_signal1)...; demean=true, fs=fs,
freq_range = (0, 5000))
out = DSP.allocate_output(config)

coh = (mt_coherence!(out, two_signal1, config))

pcoher=plot(coh.freq,coh.coherence[2,1,:],xlabel="Frequency
(Hz)",ylabel=("Coherence"),label=("S2"), line=(:red, 0.5, 6, :solid),lw=0.02,grid=false,
xtickfontsize=16,ytickfontsize=16,xguidefontsize=16,yguidefontsize=16,framestyle=:box )
#write data to xlsfile

ampfill=[amp; fill(missing, (length(Trcoeff) - length(mc_prop.freq)))];
freqfill1=[mc_prop.freq[:]; fill(missing, (length(Trcoeff) - length(mc_prop.freq)))];
freqfill2=[coh.freq[:]; fill(missing, (length(Trcoeff) - length(coh.freq)))];
coh2=coh.coherence[2,1,:];
cohfill=[coh2; fill(missing, (length(Trcoeff) - length(coh2)))]; pvfill=[phaseVel; fill(missing,
(length(Trcoeff) - length(phaseVel)))];
df =
DataFrame(frequency=frfin[:],Amp1=Trcoeff[:],pv=pvfill,frequency2=freqfill1,Amp2=ampfi
ll,frequency3=freqfill2,coherence=cohfill);
#ampfill=[; fill(missing, (length(Trcoeff) - length(coh.freq)))]; #df =
DataFrame(frequeny=frfin[:],Amp1=Trcoeff[:]);
XLSX.writetable("S 1_trcoeff.xlsx", df, overwrite=true, sheetname="transcoeff",
anchor_cell="A1");
#XLSX.writetable("S1_trcoeff.xlsx", df, overwrite=true, sheetname="transcoeff1",
```

```
anchor_cell="A2");
#df = DataFrame(frequency=mc_prop.freq[:],Amp=amp[:])

#XLSX.writetable("S1_trcoeffTP.xlsx", df, overwrite=true, sheetname="transcoeff2",
anchor_cell="A2");
#out = DSP.mt_coherence!(dt, sig1, sig2, tbp, kspec, nf, p, freq=true,cohe=true, iadapt=1)
#out=DSP.mt_coherence!(dt,sig1,sig2)
#fs2=fs;
#periodogram(sig1; onesided=eltype(sig1)<:Real, fs=fs2, window=nothing)

#mc_prop=mt_cross_power_spectra(two_signal; demean=true, fs=fs, freq_range = (0, 5000));
# test in-place gets the same result
```

APPENDIX III: SCRIPT TO PLOT ALL ACOUSTICAL PARAMETERS

```
using DelimitedFiles,XLSX ENV["GKS_ENCODING"] = "utf-8"
using Plots, LaTeXStrings, Latexify using DataFrames
global df0 = DataFrame(XLSX.readtable("All_acoustparamsV0105.xlsx", "Feuil1")...);

plot(df0[1:4:end,1], df0[1:4:end,2],line=(:blue, 0.5, 3, :solid),marker = (:rect),grid=false,label

= "0% WHA")

plot!(df0[2:4:end,1], df0[2:4:end,2],line=(:red, 0.5, 3, :dashdot),marker =
(:rtriangle),lw=0.01,grid=false,label = "3% WHA")
plot!(df0[3:4:end,1], df0[3:4:end,2],line=(:black, 0.5, 3, :dash),marker =
(:star5),lw=0.01,grid=false,label = "5% WHA")
ppor=plot!(df0[4:4:end,1], df0[4:4:end,2],xlabel="Presure (bar)",ylabel=("Φ"),line=(:green,

0.5, 3, :dot),label = "7% WHA",marker = (:circle),lw=0.01,grid=false)
#global df0 = DataFrame(XLSX.readtable("All_acoustparamsV0105.xlsx", "Feuil1")...);
plot(df0[1:4:end,1], df0[1:4:end,3],line=(:blue, 0.5, 3, :solid),marker = (:rect),grid=false,label
= "0% WHA")

plot!(df0[2:4:end,1], df0[2:4:end,3],line=(:red, 0.5, 3, :dashdot),marker =
(:rtriangle),lw=0.01,grid=false,label = "3% WHA")
plot!(df0[3:4:end,1], df0[3:4:end,3],line=(:black, 0.5, 3, :dash),marker =
(:star5),lw=0.01,grid=false,label = "5% WHA")

psig=plot!(df0[4:4:end,1], df0[4:4:end,3],xlabel="Presure (bar)",ylabel="σ",line=(:green, 0.5,
3, :dot),label = "7% WHA",marker = (:circle),lw=0.01,grid=false)
plot(df0[1:4:end,1], df0[1:4:end,4],line=(:blue, 0.5, 3, :solid),marker = (:rect),grid=false,label
= "0% WHA")
plot!(df0[2:4:end,1], df0[2:4:end,4],line=(:red, 0.5, 3, :dashdot),marker =
(:rtriangle),lw=0.01,grid=false,label = "3% WHA")
plot!(df0[3:4:end,1], df0[3:4:end,4],line=(:black, 0.5, 3, :dash),marker =
(:star5),lw=0.01,grid=false,label = "5% WHA")
```

```
pLam=plot!(df0[4:4:end,1], df0[4:4:end,4],xlabel="Presure (bar)",ylabel="Λ",line=(:green,
0.5, 3, :dot),label = "7% WHA",marker = (:circle),lw=0.01,grid=false)
plot(df0[1:4:end,1], df0[1:4:end,5],line=(:blue, 0.5, 3, :solid),marker = (:rect),grid=false,label
= "0% WHA")
plot!(df0[2:4:end,1], df0[2:4:end,5],line=(:red, 0.5, 3, :dashdot),marker =
(:rtriangle),lw=0.01,grid=false,label = "3% WHA")
plot!(df0[3:4:end,1], df0[3:4:end,5],line=(:black, 0.5, 3, :dash),marker =
(:star5),lw=0.01,grid=false,label = "5% WHA")
ptort=plot!(df0[4:4:end,1], df0[4:4:end,5],xlabel="Presure (bar)",ylabel="α",line=(:green,
0.5, 3, :dot),label = "7% WHA",marker = (:circle),lw=0.01,grid=false)
plot(df0[1:4:end,1], df0[1:4:end,6],line=(:blue, 0.5, 3, :solid),marker = (:rect),grid=false,label
= "0% WHA")
plot!(df0[2:4:end,1], df0[2:4:end,6],line=(:red, 0.5, 3, :dashdot),marker =
(:rtriangle),lw=0.01,grid=false,label = "3% WHA")

plot!(df0[3:4:end,1], df0[3:4:end,6],line=(:black, 0.5, 3, :dash),marker =
(:star5),lw=0.01,grid=false,label = "5% WHA")
pratio=plot!(df0[4:4:end,1], df0[4:4:end,6],xlabel="Presure (bar)",ylabel="Λp/Λ",line=(:green,
0.5, 3, :dot),label = "7% WHA",marker = (:circle),lw=0.01,grid=false)
plot(df0[1:4:end,1], df0[1:4:end,7],line=(:blue, 0.5, 3, :solid),marker = (:rect),grid=false,label

= "0% WHA")
plot!(df0[2:4:end,1], df0[2:4:end,7],line=(:red, 0.5, 3, :dashdot),marker =
(:rtriangle),lw=0.01,grid=false,label = "3% WHA")
plot!(df0[3:4:end,1], df0[3:4:end,7],line=(:black, 0.5, 3, :dash),marker =
(:star5),lw=0.01,grid=false,label = "5% WHA")
pkp0=plot!(df0[4:4:end,1], df0[4:4:end,7],xlabel="Presure (bar)",ylabel="kp0",line=(:green, 0.5,
3, :dot),label = "7% WHA",marker = (:circle),lw=0.01,grid=false)
plot(ppor,psig,pLam,ptort,pratio,pkp0)
```

APPENDIX IV: SCRIPT TO PLOT COST FUNCTIONS OF VARIOUS PARAMETERS

```
using DelimitedFiles,XLSX ENV["GKS_ENCODING"] = "utf-8"
using Plots, LaTeXStrings, Latexify using DataFrames
using PyCall
np = pyimport("numpy")
function coeffTrans( fr,por, resist, lambd,rapp, alphinf, k00p,d) #d = 0.2e-1;
#fr=range(0,step=10,stop=1000); w = (2*pi.*fr);
yy = 1.401;
Pr = .713;
P0 = 101325.;
rho0 = 1.297;
c0 = 344;
Kf0 = yy*P0; visc0 = 0.178e-4;
lambdp = rapp*lambd;
k00 = visc0/resist;
Gw2 = sqrt.(1 .+(4.0*im)*k00p^2*rho0.*w*Pr/(visc0*por^2*lambdp^2)); bet = yy .-(yy-1)./(1 .-
im*visc0*por.*Gw2./(w*rho0*k00*Pr));
Kf = Kf0./bet;
Gw1 = sqrt.(1 .+(4.0*im)*alphinf.^2*k00^2*rho0.*w/(visc0*por^2*lambd^2)); alphtort =
(alphinf.*(1 .-im*visc0*por.*Gw1./(w*alphinf*rho0*k00)));
k0 = w./c0;
rho2 = (rho0.*alphtort); c11 = (sqrt.(Kf./rho2)); k2 = w./c11;
z0 = rho0*c0; z2 = rho2.*c11; Z = z2./z0;
return (2*por*Z.*exp.(im*k0*d)./((2)*por.*Z.*cos.(k2*d) .+im*(por^2 .+Z.^2).*sin.(k2*d)));
end
function main()
#Initialization of porous parameters #por0 = 0.73; resist0 = 17000; #lambd0 = 2.72e-5;  alphinf0
= 2.18;
#k00p0 =1.67e-8;           rapp0=1.75;#lambdp/lambda
por0 =  0.205; resist0 = 181500; lambd0 = 1.54e-5;  alphinf0 =  1.89;
k00p0 =1.3e-9;           rapp0=1.88;#lambdp/lambda d=2.0e-2; # thickness
#Read experimental data TC from the file generated by the other program global df0 =
DataFrame(XLSX.readtable("S13_trcoeff.xlsx", "transcoeff2")...); #global xf
=XLSX.openxlsx("S4_trcoeff.xlsx",enable_cache=false) #freq=range(0,step=10,stop=3500);
```

```
freq=df0[1:11,1];#an array of frequencies where to compute if freq[1] == 0
freq[1]=0.001;
end
global AmpExp=df0[1:11,2]; #
fcoutp=[]; vpor=[];
for poro = 0.05:0.005:0.4
coeftr=coeffTrans(freq,poro,resist0, lambd0, rapp0,alphinf0, k00p0,d) fc=sum((abs.(coeftr) .-
AmpExp).^2);
push!(fcoutp,fc);
   push!(vpor,poro); end
mpor=vpor[argmin(fcoutp)] #
fcoutr=[]; vres=[];
for resist1 =150000:500:250000
coeftr=coeffTrans(freq,por0,resist1, lambd0, rapp0,alphinf0, k00p0,d) fc=sum((abs.(coeftr) .-
AmpExp).^2);
push!(fcoutr,fc); push!(vres,resist1);
 end mresist=vres[argmin(fcoutr)] #
fcoutt=[]; tort=[];
                                                                    for tortu =1:0.01:4
   --------------------
coeftr=coeffTrans(freq,por0,resist0, lambd0, rapp0,tortu, k00p0,d) fc=sum((abs.(coeftr) .-
AmpExp).^2);
                                                                      push!(fcoutt,fc);

   push!(tort,tortu); end
 mtor=tort[argmin(fcoutt)]; #
fcoutlamb=[]; lambd=[];
for lambd1 =2e-6:0.2e-6 :120e-6
coeftr=coeffTrans(freq,por0,resist0, lambd1, rapp0,alphinf0, k00p0,d) fc=sum((abs.(coeftr) .-
AmpExp).^2);
push!(fcoutlamb,fc); push!(lambd,lambd1);
 end mlambd=lambd[argmin(fcoutlamb)] #
fcoutratio=[]; ratiol=[];
for ratios =1:0.01 :3.5
```



```
   --------------------
```

```
coeftr=coeffTrans(freq,por0,resist0, lambd0, ratios,alphinf0, k00p0,d) fc=sum((abs.(coeftr) .-
AmpExp).^2);
push!(fcoutratio,fc);
   push!(ratiol,ratios); end
 mratio=ratiol[argmin(fcoutratio)] #
#  --------------------
    --------------------
 fcoutkp0=[]; kp0=[];
for kpz =5e-10:1e-10 :20e-9
coeftr=coeffTrans(freq,por0,resist0, lambd0, rapp0,alphinf0, kpz,d) fc=sum((abs.(coeftr) .-
AmpExp).^2);
push!(fcoutkp0,fc); push!(kp0,kpz);
 end mkp0=kp0[argmin(fcoutkp0)] #
global pfcoutkp0=plot(kp0,fcoutkp0,xlabel="k'0",ylabel=("Cost Function"),label=("k'_0 min
= $mkp0"),line=(:red, 0.5, 6, :solid))

   --------------------
global pfcoutpor=plot(vpor,fcoutp,xlabel="Φ",ylabel=("Cost
Function"),label=("Porosity"),line=(:red, 0.5, 6, :solid))
global pfcoutres=plot(vres/1000,fcoutr,xlabel="σ (x10^3)",ylabel=("Cost

Function"),label=("Resistivity"),line=(:red, 0.5, 6, :solid))
global pfcoutt=plot(tort,fcoutt,xlabel="α",ylabel=("Cost
Function"),label=("Tortuosity"),line=(:red, 0.5, 6, :solid))
global pfcoutlamb=plot(lambd*1e6,fcoutlamb,xlabel="Λ (x10^-6)",ylabel=("Cost
Function"),label=("Lambda"),line=(:red, 0.5, 6, :solid))
global pfcoutratio=plot(ratiol,fcoutratio,xlabel="Λ'/Λ",ylabel=("Cost
Function"),label=("Ratio"),line=(:red, 0.5, 6, :solid))
global ptc=plot(freq,AmpExp,ylims=(0,1),xlabel="Frequency
(Hz)",ylabel=("|T|"),legend=:topright,line=(:blue, 0.5, 6, :dash),marker =
(:star5),lw=0.01,grid=false, label
=("Experiment"),xtickfontsize=16,ytickfontsize=16,xguidefontsize=16,yguidefontsize=16,fra
mestyle=:box )
fr=1:50:4000;
coeftr=coeffTrans(fr,por0,resist0, lambd0, rapp0,alphinf0, k00p0,d) AmpTH=abs.(coeftr);
```

```
global ptct=plot!(fr,AmpTH,ylims=(0,1),xlabel="Frequency
(Hz)",ylabel=("|T|"),legend=:topright,line=(:red, 0.5, 6, :solid),marker =
(:hex),lw=0.02,grid=false, label
=("Model"),xtickfontsize=16,ytickfontsize=16,xguidefontsize=16,yguidefontsize=16,framest
yle=:box )
#  ----------------------

#Saving variables to xlsx file #
l1=length(vpor); l2=length(vres); l3=length(tort); l4=length(lambd); l5=length(ratiol);
l6=length(kp0); l7=length(freq); l8=length(fr);
global lmx= findmax([l1 l2 l3 l4 l5 l6])[1]# find max length #lmx= findmax([l7 l8])[1]# find
max length
#create arrays of equal length vpor=[vpor; fill(missing, (lmx-l1)) ]; fcoutp=[fcoutp; fill(missing,
(lmx-l1)) ]; vres=[vres; fill(missing, (lmx-l2)) ]; fcoutr=[fcoutr; fill(missing, (lmx-l2)) ];
tort=[tort; fill(missing, (lmx-l3)) ]; fcoutt=[fcoutt; fill(missing, (lmx-l3))];
lambd=[lambd; fill(missing, (lmx-l4)) ];

fcoutlamb=[fcoutlamb; fill(missing, (lmx-l4)) ]; ratiol=[ratiol; fill(missing, (lmx-l5)) ];
fcoutratio=[fcoutratio; fill(missing, (lmx-l5)) ]; kp0=[kp0; fill(missing, (lmx-l6)) ];
fcoutkp0=[fcoutkp0; fill(missing, (lmx-l6)) ];
global df1 =
DataFrame(por=[por0,mpor],resist=[resist0,mresist],tort=[alphinf0,mtor],lambda=[lambd0,ml
ambd],ratio=[rapp0,mratio], kp0=[k00p0,mkp0]);
df2 = DataFrame(vpor=vpor,fc_por=fcoutp, vres=vres,fcout_res=fcoutr,tort=tort, fc_tort=fcoutt,
lambda=lambd, fc_lamb=fcoutlamb,ratio=ratiol,fc_ratio=fcoutratio, kp0=kp0,fc_kp0=fcoutkp0);
#  ------------------------

#saving reconstructed and original data #
 lmx= findmax([l7 l8])[1]# find max length global fr_exp=[freq; fill(missing, (lmx-l7))];
Amp_Exp=[AmpExp; fill(missing, (lmx-l7))]; global fr_th=[fr; fill(missing, (lmx-l8))];
global Amp_th=[AmpTH; fill(missing, (lmx-l8))]; global df3 = DataFrame(frTh=fr_th,
AmpTh=Amp_th);

#df = DataFrame(frequeny=frfin[:],Amp1=Trcoeff[:]);
#XLSX.writetable("S6_acoustparams.xlsx", df, overwrite=true, sheetname="transcoeff1",
```

```
anchor_cell="A1");
XLSX.writetable("S13_acoustparamsV3.xlsx",overwrite=true, REPORT_A=(
collect(DataFrames.eachcol(df1)), DataFrames.names(df1) ), REPORT_B=(
collect(DataFrames.eachcol(df2)), DataFrames.names(df2) ),
REPORT_C=( collect(DataFrames.eachcol(df0)), DataFrames.names(df0) ), REPORT_D=(
collect(DataFrames.eachcol(df3)), DataFrames.names(df3) )) rho0 = 1.297;
Pr = .713;
visc0 = 0.178e-4;
global FC=resist0*por0/(2*pi*alphinf0*rho0); global FpC=visc0*por0/(2*pi*rho0*k00p0*Pr)
end
main()
#in the command line to plot all the cost functions
global fcs=plot( pfcoutpor,pfcomb,pfcoutt,pfcoutres,pfcoutratio,pfcoutkp0)
```